Progress In Electromagnetics Research, Vol. 127, 211–257, 2012

AN EFFICIENT METHOD FOR COMPUTING HIGHLY OSCILLATORY PHYSICAL OPTICS INTEGRAL

Y. M. Wu[1], L. J. Jiang[1], and W. C. Chew[2,*]

[1]Department of Electric and Electronic Engineering, The University of Hong Kong, Pokfulam Road, Hong Kong SAR

[2]Department of Electrical and Computer Engineering, University of Illinois at Urbana-Champaign, (on part-time appointment with HKU), Urbana, IL 61801, USA

Abstract—In this work, we use the numerical steepest descent path (numerical SDP) method in complex analysis theory to calculate the highly oscillatory physical optics (PO) integral with quadratic phase and amplitude variations on the triangular patch. The Stokes' phenomenon will occur due to various asymptotic behaviors on different domains. The stationary phase point contributions are carefully studied by the numerical SDP method and complex analysis using contour deformation. Its result agrees very well with the leading terms of the traditional asymptotic expansion. Furthermore, the resonance points and vertex points contributions from the PO integral are also extracted. Compared with traditional approximate asymptotic expansion approach, our method has significantly improved the PO integral accuracy by one to two digits (10^{-1} to 10^{-2}) for evaluating the PO integral. Moreover, the computation effort for the highly oscillatory integral is frequency independent. Numerical results for PO integral on the triangular patch are given to verify the proposed numerical SDP theory.

1. INTRODUCTION

When the electrical size of objects are on the order of hundreds or thousands of working wavelength λ, that is, the essential frequencies k of the wave field are high enough, the *physical optics* (PO) approximation has been accepted as an efficient approach for analyzing the scattering and radiation electromagnetic problems [2–14, 16–19],

Received 23 February 2012, Accepted 2 April 2012, Scheduled 16 April 2012

* Corresponding author: Weng Cho Chew (w-chew@uiuc.edu).

which was suggested by Macdonald [4] early in 1913. The PO current on a scattering surface *lit region* is defined by

$$j_{\mathrm{PO}}^{(s)}(\mathbf{r}) = 2\frac{\partial u^{(i)}(\mathbf{r})}{\partial n}, \quad j_{\mathrm{PO}}^{(h)}(\mathbf{r}) = 2u^{(i)}(\mathbf{r}), \tag{1}$$

$$\mathbf{J}_{\mathrm{PO}}(\mathbf{r}) = 2\hat{\mathbf{n}} \times \mathbf{H}^{(i)}(\mathbf{r}), \tag{2}$$

where $u^{(i)}(\mathbf{r})$ is the incident wave, $j_{\mathrm{PO}}^{(s)}$ and $j_{\mathrm{PO}}^{(h)}$ are the scalar acoustic currents due to the soft ($u|_{\partial\Omega} = 0$) and hard ($(\partial u/\partial n)|_{\partial\Omega} = 0$) boundary conditions, respectively. $\mathbf{J}_{\mathrm{PO}}$ defined in Equation (2) is the electromagnetic wave current in the lit region. In the *shadow region* of the scattering surface $\partial\Omega$, this PO current is set to zero. Due to the soft boundary condition, the acoustic scattered field integral by PO expression is:

$$u_{\mathrm{PO}}^{(s)}(\mathbf{r}) = -\int_{\partial\Omega_1} j_{\mathrm{PO}}^{(s)}(\mathbf{r}')g(\mathbf{r},\mathbf{r}')ds(\mathbf{r}'), \quad g(\mathbf{r},\mathbf{r}') = \frac{1}{4\pi}\frac{e^{ik|\mathbf{r}-\mathbf{r}'|}}{|\mathbf{r}-\mathbf{r}'|}, \tag{3}$$

where $\partial\Omega_1$ is the lit surface of the scatterer and $g(\mathbf{r},\mathbf{r}')$ is the scalar Green's function in the homogeneous medium. For electromagnetic waves, the PO integral has the similar expression as Equation (3), but we shall use the dyadic Green's function [1]. To guarantee that the PO approximation is accurate enough for the full-wave scattering, the observation point $\mathbf{r}$ shall be far away from the scatterer's *shadow and reflection boundaries* [3, 21, 22]. In this situation, the PO scattered field integral can be represented by a surface integral:

$$I = \int_{\partial\Omega} s(\mathbf{r})e^{ikv(\mathbf{r})}ds, \tag{4}$$

where $s(\mathbf{r})$ is a slowly varying amplitude function, and the exponent of the phase function term, i.e., $e^{ikv(\mathbf{r})}$ will become highly oscillatory as the frequency k increases. Hence, the PO integral kernel is getting more oscillatory as the electrical size of object becomes larger compared with the incident wavelength λ. Consequently, the computational cost by a direct numerical integration scheme [12, 20] for the PO integral is extremely high.

Due to the importance and challenges of acoustic, elastic and electromagnetic waves in high frequency applications, efficient numerical methods have attracted much attentions from mathematicians [23–29]. Bruno et al. employed the full-wave combined-field boundary integral formulation and asymptotic theories to solve this type of problems. It is the extension of the stationary phase method for convex and smooth obstacles [24–26], where the ideas of asymptotic theories are incorporated into the localized integration method. Engquist and Runborg [28, 29] considered the traditional ray tracing technique based on

the variant of *geometrical optics* (GO). It is obtained by the asymptotic approximations when the wave field frequency tends to infinity. Furthermore, the eikonal equation and the approximation of the Liouville equation based on GO have been employed for simulating the high frequency wave propagation.

Traditional asymptotic expansion approximations [3, 18, 38–43] are widely used in computational electromagnetics, optics, acoustics and geophysics areas. The asymptotic expansion approximation for the highly oscillatory PO integral [10, 17–19] is a frequency-independent approach. However, it generally leads to limited accuracy, especially when the object is not very large. These challenging PO type oscillatory integrals are extensively studied in [30–37]. Relevant mathematical theories and error analysis are developed to provide clearer pictures about their oscillatory behaviors. Some comprehensive numerical quadratures, such as Filon-type and Levin-type methods, are developed by the aid of the asymptotic approximate expansion approach. The SDP or numerical SDP [37, 45] techniques in the complex plane [1, 17] is very efficient in computing highly oscillatory integrals by the steepest descent integral path deformation. Since less approximation is done compared with the traditional asymptotic expansion, the numerical SDP method opens up a hopeful way in computing PO integrals frequency independently and error controllably.

Analytical expressions for reducing the highly oscillatory double PO integral to a line integral were given by Gordon [6, 7]. Based on the standard far-field approximation, the Kirchhoff formula was used for the scattered field under the assumption that the amplitude and phase functions vary linearly. Then closed form formulas were obtained on flat patches. In [8–10], Ergin used the radon transform to develop the closed form expression of the PO integral on the triangular patch and even NURBS surface, the proposed method is efficient for electromagnetic scattering problems. Cátedra et al. [15] and Vico et al. [17] extended the phase and amplitude variation by using quadratic functions. Different approximated closed forms were developed from it. In [17], the PO integral on a surface is presented by a decomposition of the surface into small triangles. In each triangle, a path deformation in the complex plane is used to accelerate the integration.

The proposed numerical steepest descent path method in this manuscript comes from the physical meaning of the PO integral. Physically, we know the dominant terms of the PO integral shall be the stationary phase point contribution, which agrees well with geometry optics (GO) theory. In order to capture the stationary phase point contribution, we consider the phase function with quadratic

variation. Once the stationary phase point exists in the PO integrand, the resonance point contribution and Stokes' phenomenon related to the reflection and shadow boundaries of GO theory can also be captured. For the PO integrand with linear phase variation, the stationary phase point does not exist. And the size of $\lambda/10$ meshes shall be used to compute the PO integral while the mesh size does not dependent on the wavelength by the quadratic phase variation. In this paper, the starting problem is similar to [17]. We deal with highly oscillatory PO integrals with the quadratic variation of amplitude and phase functions on triangular patches. Double integrals are reduced into line integrals in terms of complementary error functions. For each linear integral, the numerical SDP method and *Stokes lines* are used to achieve the frequency independency in computing the highly oscillatory line integral. Compared with [17], our new contributions in this paper are: Stokes lines are comprehensively studied to extract the *stationary phase point* (SPP) contributions; *Resonance point* and *vertex point* contributions are also exactly extracted, and compared with the asymptotic results in [18]; Cancellation of the internal resonance and vertex points contributions are mathematically proved when we assemble triangle meshes together for practical engineering applications. Thus, we just need to consider the triangle patches that contain the stationary phase point, the boundary resonance points, and the boundary vertex points. Thus, the number of considered triangles shall be significantly reduced for the realistic objects. New mathematical theories and formulas for all cases of PO integrals on edges are developed depending on the relative locations of endpoints, Stokes lines and stationary phase points. We employ the complementary error function instead of the n-repeated Fresnel function. Only two trapezoidal decompositions of each triangle are needed instead of six trapezoidal decompositions in [17]. Both improvements give rise to elegant mathematical formulas. All new derivations are verified by the brute force method and compared with the asymptotic approximation approach.

To our best knowledge, this is the first time that comparisons of the point contributions by using the numerical SDP method and traditional asymptotic approximation approach for highly oscillatory PO integrals have been given. Since the numerical SDP method uses less approximation, its numerical result is more accurate than the asymptotic approximations. Detailed numerical results and comparisons with [18] are provided. When the frequency k is around 50, our numerical SDP method can significantly improve the point contributions accuracy to one to two digits (10^{-1} to 10^{-2}), which is very valuable for engineering. Moreover, the computation efforts by

the numerical SDP method retains frequency-independent as in [44].

This paper is organized as follows: the highly oscillatory PO integral on right-angled trapezoid domains are discussed in Section 2. The two dimensional integral is reduced to several line integrals. Steepest descent paths are used and different cases PO integral formulas are given. In Section 3, we extend the PO integral to the triangular patch. Mathematical formulas of the PO integrals are decomposed as the resonance point, vertex point and stationary point physically contributions. The formulations are analyzed to compare these point contributions results with leading terms of traditional asymptotic approximation in Section 5. In Section 6, numerical results of PO integrals on a trapezoid domain and triangular patch are compared by the asymptotic approximation approach, the brute force and the numerical SDP methods. The comparisons show that the proposed numerical SDP method is error-controllable and frequency-independent. The detailed mathematical closed-form formula derivations are documented in the Appendix.

2. HIGHLY OSCILLATORY PO INTEGRALS ON THE RIGHT-ANGLE TRAPEZOID DOMAIN

In electromagnetics, the PO scattered field by an object with surface $\partial\Omega$ can be represented by a surface PO integral in Equation (4):

$$I = \int_{\partial\Omega} s(\mathbf{r}) e^{ikv(\mathbf{r})} ds,$$

where $\mathbf{r} = (x, y, z)$ is the Cartesian coordinate, $s(\mathbf{r})$ is a slowly varying amplitude function, and the exponential of the phase function, i.e., $e^{ikv(\mathbf{r})}$ will become highly oscillatory as the frequency k increases (see Figure 1).

We assume the object surface $\partial\Omega$ is given by equation $z = f(x, y)$, and the projection of $\partial\Omega$ onto x-y plane is $\partial\Omega_{xy}$. Then the domain $\partial\Omega_{xy}$ can be discretized into M triangles, Δ_1, Δ_2, ..., Δ_M. To capture the stationary phase points phenomenon and give the closed-form formulas for the PO integral I given in Equation (4), we assume the integrand of I has the quadratic variation of the amplitude and phase functions on these triangular patches. In this sense, the surface integral can be represented as

$$\begin{aligned} I &= \int_{\partial\Omega_{xy}} \tilde{s}(x,y) e^{ik\tilde{v}(x,y)} \sqrt{1 + [f_x(x,y)]^2 + [f_y(x,y)]^2}\, dxdy \\ &= \sum_{n=1}^{M} \int_{\Delta_n} \tilde{d}(x,y) e^{ik\tilde{v}(x,y)} dxdy \simeq \sum_{n=1}^{M} \int_{\Delta_n} \tilde{d}_n(x,y) e^{ik\tilde{v}_n(x,y)} dxdy, \quad (5) \end{aligned}$$

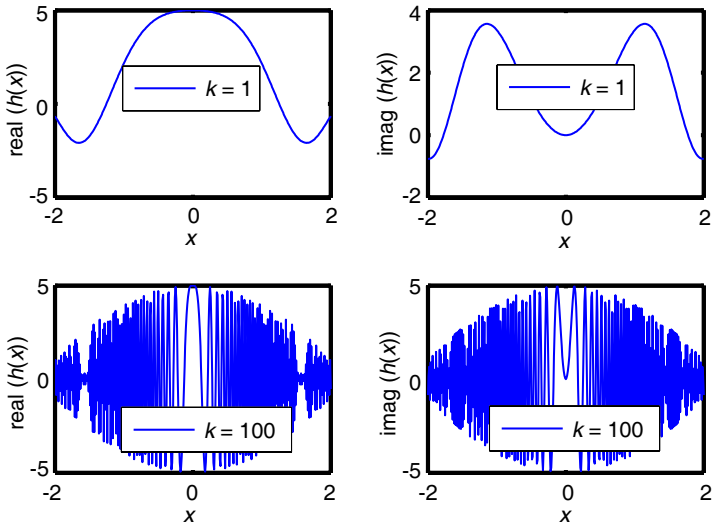

Figure 1. One example of the PO type highly oscillatory behavior with the integrand $h(x) = (5 - x^2)e^{ikx^2}$.

where

$$\tilde{s}(x,y) = s\left(x,y,f(x,y)\right), \quad \tilde{v}(x,y) = v\left(x,y,f(x,y)\right),$$
$$\tilde{d}(x,y) = \tilde{s}(x,y)\sqrt{1+\left[f_x(x,y)\right]^2+\left[f_y(x,y)\right]^2}.$$

The second order polynomials $\tilde{d}_n(x,y)$ and $\tilde{v}_n(x,y)$ are the quadratic amplitude and phase functions. They can be got by the Lagrange interpolation polynomial approximation of $\tilde{d}(x,y)$ and $\tilde{v}(x,y)$ on these triangular patches Δ_n, $n = 1, 2, \ldots, M$. Their formulas are

$$\tilde{v}_n(x,y) = \tilde{\beta}_{n,1} + \tilde{\beta}_{n,2}x + \tilde{\beta}_{n,3}y + \tilde{\beta}_{n,4}x^2 + \tilde{\beta}_{n,5}y^2 + \tilde{\beta}_{n,6}xy, \quad (6)$$
$$\tilde{d}_n(x,y) = \tilde{\alpha}_{n,1} + \tilde{\alpha}_{n,2}x + \tilde{\alpha}_{n,3}y + \tilde{\alpha}_{n,4}x^2 + \tilde{\alpha}_{n,5}y^2 + \tilde{\alpha}_{n,6}xy, \quad (7)$$

where $\tilde{\alpha}_{n,m} \in \mathbb{C}$, $\tilde{\beta}_{n,m} \in \mathbb{R}$, $m = 1, 2, \ldots, 6$.

However, the quadratic phase function $\tilde{v}_n(x,y)$ of each summation integral term in Equation (5) has the simplified canonical form. We notice that $\tilde{v}_n(x,y)$ in Equation (6) can be written in the matrix notation as

$$\begin{aligned}\tilde{v}_n(x,y) &= \begin{bmatrix} x & y \end{bmatrix} \cdot \mathbf{W}_n \cdot \begin{bmatrix} x \\ y \end{bmatrix} + \tilde{\beta}_{n,2}x + \tilde{\beta}_{n,3}y + \tilde{\beta}_{n,1}, \\ &= \begin{bmatrix} x-\tilde{a}_n & y-\tilde{c}_n \end{bmatrix} \cdot \mathbf{W}_n \cdot \begin{bmatrix} x-\tilde{a}_n \\ y-\tilde{c}_n \end{bmatrix} + \tilde{G}_n, \end{aligned} \quad (8)$$

where the symmetric matrix $\mathbf{W}_n$ has the form

$$\mathbf{W}_n = \begin{bmatrix} \tilde{\beta}_{n,4} & \frac{\tilde{\beta}_{n,6}}{2} \\ \frac{\tilde{\beta}_{n,6}}{2} & \tilde{\beta}_{n,5} \end{bmatrix}.$$

We consider the case that the eigenvalues of $\mathbf{W}_n$ are not zero (nondegenerate). If we assume $\tilde{G}_n$ is a constant in Equation (8), then the coefficients $\tilde{a}_n$ and $\tilde{c}_n$ can be uniquely found by the relationships

$$\begin{aligned} \tilde{\beta}_{n,2} + 2\tilde{\beta}_{n,4}\tilde{a}_n + \tilde{\beta}_{n,6}\tilde{c}_n &= 0, \\ \tilde{\beta}_{n,3} + 2\tilde{\beta}_{n,5}\tilde{c}_n + \tilde{\beta}_{n,6}\tilde{a}_n &= 0. \end{aligned}$$

After getting $\tilde{a}_n$ and $\tilde{c}_n$, the coefficient $\tilde{G}_n$ in Equation (8) has the formula

$$\tilde{G}_n = -\left(\tilde{\beta}_{n,4}\tilde{a}_n^2 + \tilde{\beta}_{n,5}\tilde{c}_n^2 + \tilde{\beta}_{n,6}\tilde{a}_n\tilde{c}_n - \tilde{\beta}_{n,1}\right).$$

Since $\mathbf{W}_n$ is a nondegenerate symmetric matrix, we can always find the invertible congruent transformation matrix

$$\mathbf{Q}_n = \begin{bmatrix} \mathbf{q}_{n,1} & \mathbf{q}_{n,2} \end{bmatrix} = \begin{bmatrix} q_{n,11} & q_{n,12} \\ q_{n,21} & q_{n,22} \end{bmatrix},$$

such that

$$\mathbf{Q}_n^T \cdot \mathbf{W}_n \cdot \mathbf{Q}_n = \mathbf{D}_n = \begin{bmatrix} \chi_{n,1} & \\ & \chi_{n,2} \end{bmatrix}, \tag{9}$$

with $\chi_{n,j} = 1$ or -1, $j = 1, 2$. Also, the coefficient $\tilde{G}_n$ in Equation (8) can always be written as (not unique)

$$\tilde{G}_n = \begin{bmatrix} g_{n,1} & g_{n,2} \end{bmatrix} \cdot \mathbf{D}_n \cdot \begin{bmatrix} g_{n,1} & g_{n,2} \end{bmatrix}^T. \tag{10}$$

Combining Equations (8)–(10), and after the coordinate transform

$$\begin{bmatrix} x' \\ y' \end{bmatrix} = \mathbf{Q}_n^{-1} \cdot \begin{bmatrix} x - \tilde{a}_n \\ y - \tilde{c}_n \end{bmatrix} + \begin{bmatrix} g_{n,1} \\ g_{n,2} \end{bmatrix}, \tag{11}$$

the quadratic phase function $\tilde{v}_n(x, y)$ in Equation (6) can be simplified as its canonical form:

$$\tilde{v}_n(x', y') = \chi_{n,1}(x')^2 + \chi_{n,2}(y')^2, \text{ with } \chi_{n,j} = 1 \text{ or } -1,\ j = 1, 2. \tag{12}$$

Since the coordinate transform in Equation (11) is an affine transformation, it will always map the triangle Δ_n to another triangle Δ'_n. Each summation integral term in Equation (5) can be written as

$$\int_{\Delta'_n} \tilde{p}_n(x', y') e^{ik\left[\pm(x')^2 \pm (y')^2\right]} dx'dy', \tag{13}$$

where $\tilde{p}_n(x', y')$ is the multiplication of function $\tilde{d}_n(x, y)$ in x'-y' coordinate system and the determination of Jacobi coordinate transform matrix $\partial(x, y)/\partial(x', y')$.

To study the above simplified PO integral as shown in Equation (13), in this paper, we focus on the canonical PO integral

$$I = \int_{\Delta} p(x, y) e^{ik(x^2+y^2)} ds, \tag{14}$$

where Δ is an arbitrary triangle. The second order polynomial $p(x, y)$ has the form

$$p(x, y) = \alpha_1 + \alpha_2 x + \alpha_3 y + \alpha_4 x^2 + \alpha_5 y^2 + \alpha_6 xy, \tag{15}$$

where $\alpha_m \in \mathbb{C}$, $m = 1, 2, \ldots, 6$.

Direct numerical scheme such as the adaptive Simpson's rule for evaluating the above integral I is time-consuming for high frequency k. In other words, the number of discretized triangles $M = M(k) \sim O(k^2)$ in Equation (5). In the following, we derive a k-independent formula on a right-angle trapezoid domain.

2.1. Reduction of the Double Integral into the Line Integrals

We first consider the highly oscillatory integrand $p(x, y)e^{ik(x^2+y^2)}$ defined on the domain $[L_1, L_2] \times [0, ax + b]$ as shown in Figure 2. It can be written as

$$I = \int_{L_1}^{L_2} \int_{0}^{ax+b} p(x, y) e^{ik(x^2+y^2)} dy dx = \int_{L_1}^{L_2} e^{ikx^2} F(x) dx, \tag{16}$$

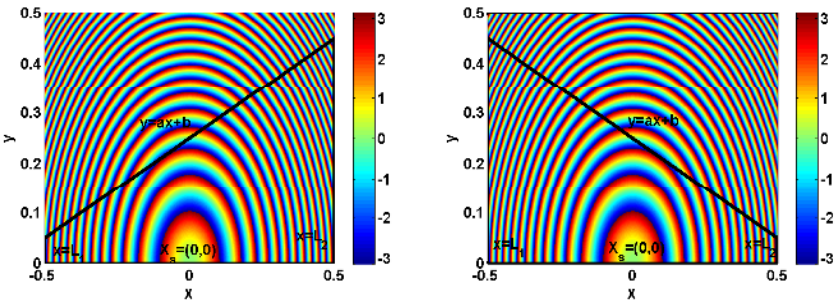

Figure 2. Integration domains $[L_1, L_2] \times [0, ax + b]$ for the highly oscillatory integrand given in Equation (16), (a) $a > 0$, (b) $a < 0$.

here we assume $ax + b > 0$, and

$$\begin{aligned} F(x) &= \int_0^{ax+b} p(x,y)e^{iky^2}dy \\ &= -\frac{\sqrt{\pi}}{2\sqrt{-ik}}\left(\alpha_1+\alpha_2 x+\alpha_4 x^2-\frac{\alpha_5}{2ik}\right)\left(\mathrm{erfc}\left(\sqrt{-ik}(ax+b)\right)-1\right) \\ &\quad +\frac{\alpha_3+\alpha_6 x+\alpha_5(ax+b)}{2jk}e^{ik(ax+b)^2}-\frac{\alpha_3+\alpha_6 x}{2ik}, \end{aligned} \tag{17}$$

(see Appendix A), where the complementary error function $\mathrm{erfc}\,(z)$ is defined by

$$\mathrm{erfc}(z) = \frac{2}{\sqrt{\pi}}\int_z^\infty e^{-t^2}dt, \quad \text{and} \quad \mathrm{erfc}(0) = 1.$$

On the other hand, $F(x)$ in Equation (17) can be decomposed into two different parts defined on edge $y = 0$ and edge $y = ax + b$. They are $J_1(x)$ and $J_2^{(a,b)}(x)$, respectively:

$$F(x) = J_2^{(a,b)}(x) - J_1(x), \tag{18}$$

where

$$J_1(x) = \frac{\alpha_3+\alpha_6 x}{2ik} - \frac{\sqrt{\pi}}{2\sqrt{-ik}}\left(\alpha_1+\alpha_2 x+\alpha_4 x^2-\frac{\alpha_5}{2ik}\right), \tag{19}$$

$$J_2^{(a,b)}(x) = j_1(x)\mathrm{erfc}\left(\sqrt{-ik}(ax+b)\right) + j_2^{(a,b)}(x)e^{ik(ax+b)^2}, \tag{20}$$

with

$$\begin{aligned} j_1(x) &= -\frac{\sqrt{\pi}}{2\sqrt{-ik}}\left(\alpha_1+\alpha_2 x+\alpha_4 x^2-\frac{\alpha_5}{2ik}\right), \\ j_2^{(a,b)}(x) &= \frac{\alpha_3+\alpha_6 x+\alpha_5(ax+b)}{2ik}. \end{aligned}$$

Thus the original integral I in Equation (16) can be rewritten as

$$\begin{aligned} I &= \int_{L_1}^{L_2}\int_0^{ax+b} p(x,y)e^{ik(x^2+y^2)}dydx \\ &= \int_{L_1}^{L_2}\left(J_2^{(a,b)}(x) - J_1(x)\right)e^{ikx^2}dx = I_2 - I_1, \end{aligned} \tag{21}$$

where

$$I_1 = \int_{L_1}^{L_2} J_1(x)e^{ikx^2}dx, \quad I_2 = \int_{L_1}^{L_2} J_2^{(a,b)}(x)e^{ikx^2}dx.$$

I_1 is a highly oscillatory integral, but its integrand is a holomorphic function. After integration by parts, it has the closed form formula related to special complementary error functions erfc (z) as follows:

$$I_1 = S(L_2) - S(L_1), \tag{22}$$

where

$$S(L_n) = Z_1 \text{erfc}\left(\sqrt{-ik}L_n\right) + Z_2 e^{ikL_n^2}, \tag{23}$$

with

$$\begin{aligned} Z_1 &= \left(-\frac{\pi}{4ik}\alpha_1 - \frac{\sqrt{\pi}}{4ik\sqrt{-ik}}\alpha_3 - \frac{\pi}{8k^2}\alpha_4 - \frac{\pi}{8k^2}\alpha_5\right), \\ Z_2 &= \left(-\frac{\sqrt{\pi}}{4ik\sqrt{-ik}}\alpha_2 - \frac{\sqrt{\pi}L_n}{4ik\sqrt{-ik}}\alpha_4 - \frac{1}{4k^2}\alpha_6\right), \end{aligned}$$

and index $n = 1, 2$. But I_2 is a highly oscillatory integral that cannot be solved analytically. In the following, we use the path deformation technique to deform the original integration path $[L_1,\ L_2]$ to the steepest descent path in the complex plane [1]. The power series and asymptotic expansion of the complementary error function erfc (z) [46] are respectively of the forms

$$\begin{aligned} \text{erfc}(z) &= \sum_{l=0}^{\infty} \frac{(-1)^l z^l}{2^{-l} l! \Gamma\left(1 - \frac{l}{2}\right)}, \\ \text{erfc}(z) &\sim \frac{2}{\sqrt{\pi}} \frac{e^{-z^2}}{2z} \sum_{m=0}^{\infty} \frac{(-1)^m (2m)!}{m!(2z)^{2m}}, \quad \left(z \to \infty,\ |\arg(z)| < \frac{3\pi}{4}\right), \end{aligned}$$

where "$\sim$" means "asymptotic to". When $l = 2$, the first power series term above is regarded as 0.

From Figures 3–4, we can see the oscillatory behaviors of erfc $(\sqrt{-iz})$ and e^{iz^2}. The complementary error function erfc (z) has the following features:

$$\text{erfc}\left(\sqrt{-ik}z\right) \sim \begin{cases} \zeta(z)e^{ikz^2}, & z \in \prod, \\ 2 + \varsigma(z)e^{ikz^2}, & z \in \coprod, \end{cases} \tag{24}$$

the above Equation (24) holds when $\sqrt{-ik}z \to \pm\infty$. Where $\zeta(z)$, $\varsigma(z)$ are two slowly varying functions defined on two domains $\prod$, $\coprod$ on the complex plane:

$$\begin{aligned} \prod &= \left\{ z \in \mathbb{C} :\ \text{Re}(z) + \text{Im}(z) \geq 0,\ \arg(z) \in \left[-\frac{\pi}{4}, \frac{3\pi}{4}\right] \right\}, \\ \coprod &= \left\{ z \in \mathbb{C} :\ \text{Re}(z) + \text{Im}(z) < 0,\ \arg(z) \in [-\pi, \pi] \Big\backslash \left[-\frac{\pi}{4}, \frac{3\pi}{4}\right] \right\}. \end{aligned} \tag{25}$$

The above defined asymptotic behaviors of the phases on different domains are called the Stokes' phenomenon [1]. The separated line between $\prod$ and $\coprod$ is

$$l(z): \ \mathrm{Re}(z) + \mathrm{Im}(z) = 0, \tag{26}$$

which is called the Stokes line. Substituting $z = \sqrt{k}(ax + b)$ into

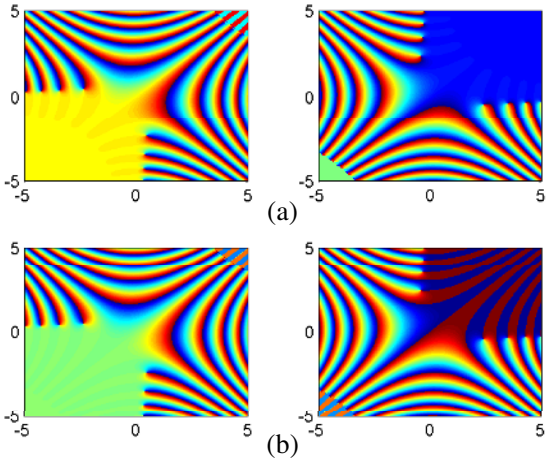

Figure 3. Oscillatory behaviors of the Fresnel function of order 0 in [17], i.e., $\mathrm{Fr}_0(z) = \frac{\sqrt{i\pi}}{2}\mathrm{erfc}(\sqrt{-iz})$ and $\mathrm{Fr}_0(z) - \sqrt{i\pi}$ (a). Oscillatory behaviors of the error function, i.e., $\mathrm{erfc}\,(\sqrt{-iz})$ and $\mathrm{erfc}\,(\sqrt{-iz}) - 2$ (b).

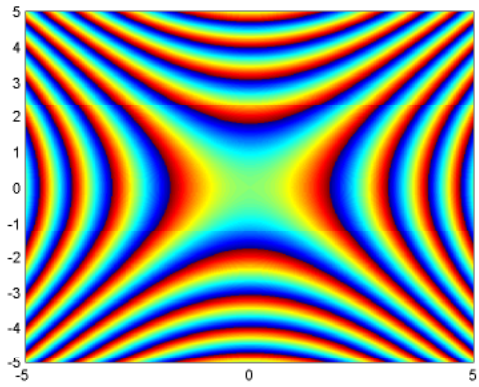

Figure 4. Oscillatory behavior of e^{iz^2}.

Equation (24), and denoting the following function:

$$E^c(x) \simeq \begin{cases} \zeta\left(\sqrt{k}(ax+b)\right), & ax+b \in \prod, \\ \varsigma\left(\sqrt{k}(ax+b)\right), & ax+b \in \coprod. \end{cases} \tag{27}$$

Then by substituting Equation (24) into Equation (20), the phase variation term of the integrand of the highly oscillatory integral I_2 is $g(x) = x^2 + (ax+b)^2$.

2.2. Numerical Steepest Descent Paths

For the highly oscillatory phase term $e^{ikg(x)}$, we notice that

$$e^{ikg(x)} = e^{ik(\mathrm{Re}(g(x))+i\mathrm{Im}(g(x)))} = e^{-k\mathrm{Im}(g(x))+ik\mathrm{Re}(g(x))}. \tag{28}$$

For a starting point L_1, if we define a path function $x = \varphi_{L_1}(p)$, $p \in [0,\infty)$ satisfying the following three conditions:

(a) $\varphi_{L_1}(0) = L_1$, that is, the path starts at L_1.
(b) $\mathrm{Re}(g(\varphi_{L_1}(p))) = \mathrm{Re}(g(\varphi_{L_1}(0))) \equiv C$, where C is a constant;
(c) $\mathrm{Im}(g(\varphi_{L_1}(p))) = p$.

After substituting $x = \varphi_{L_1}(p)$ into Equation (28), we can find that the function $e^{ikg(\varphi_{L_1}(p))} = e^{ikC-kp}$ will decrease exponentially when p goes large. Based on (b) and (c), the steepest descent path: $x = \varphi_{L_1}(p)$ can be found from the following equation:

$$g(\varphi_{L_1}(p)) = C + ip. \tag{29}$$

By setting $p = 0$ in the above equation, we get $C = g(L_1)$ from condition (a). After substituting $g(x)$ into (29), we have

$$\begin{aligned} & \varphi_{L_1}(p)^2 + (a\varphi_{L_1}(p)+b)^2 = L_1^2 + (aL_1+b)^2 + ip, \\ \Longrightarrow \quad & \varphi_{L_1}(p) = \frac{\mathrm{sign}(L_1')}{\sqrt{1+a^2}}\sqrt{{L_1'}^2 + ip} + x_s, \quad p \in [0,\infty), \end{aligned} \tag{30}$$

where $L_1' = \sqrt{1+a^2}(L_1 - x_s)$, and $x_s = -\frac{ab}{1+a^2}$ (i.e., the point x_s satisfies $g'(x_s) = 0$) is the stationary phase point of the phase function $g(x) = x^2 + (ax+b)^2$. Similarly, by substituting L_2 into (29), we have $\varphi_{L_2}(p)$ defined as follows:

$$\varphi_{L_2}(p) = \frac{\mathrm{sign}(L_2')}{\sqrt{1+a^2}}\sqrt{{L_2'}^2 + ip} + x_s, \quad p \in [0,\infty) \tag{31}$$

where $L_2' = \sqrt{1+a^2}(L_2 - x_s)$.

For the stationary phase point x_s, that is $g'(x_s) = 0$, we can see that

$$g(x) - g(x_s) \approx \frac{(x - x_s)^2}{2!} g''(x_s) + O\left((x - x_s)^3\right), \quad x \to x_s.$$

Hence, $g(x) - g(x_s)$ is quadratic around x_s [1]. So we define a path function $x = \varphi_0(p)$, $p \in (-\infty, \infty)$, such that

$$\varphi_0(p)^2 + (a\varphi_0(p) + b)^2 = x_s^2 + (ax_s + b)^2 + ip^2.$$

By substituting x_s into the above equation, we have $\varphi_0(p)$ defined as follows:

$$\varphi_0(p) = \frac{e^{\left(i\frac{\pi}{4}\right)} p}{\sqrt{1 + a^2}} + x_s, \quad p \in (-\infty, \infty). \tag{32}$$

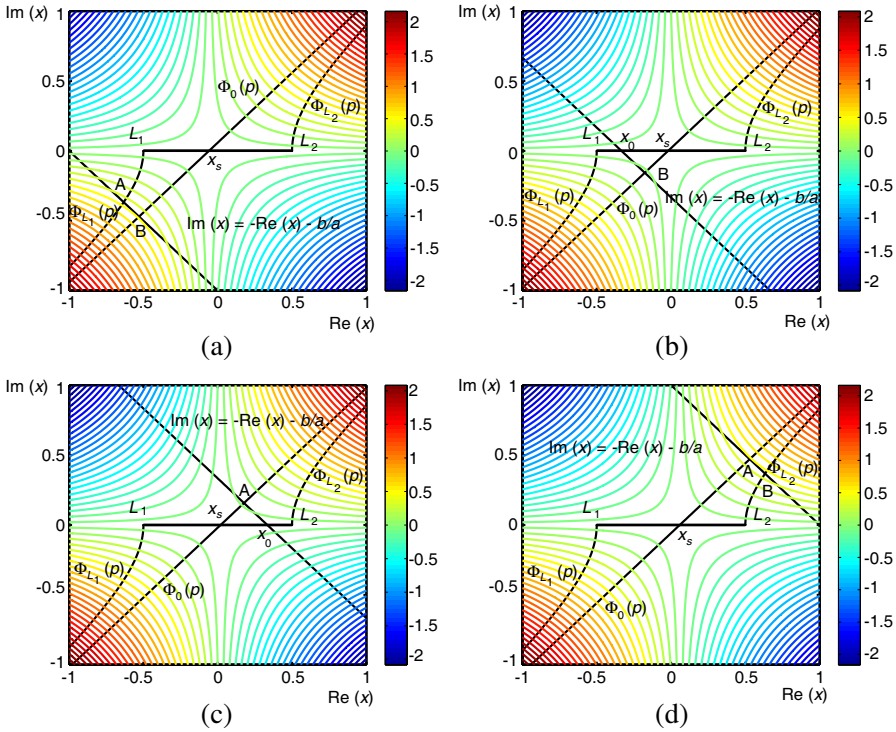

Figure 5. Contour curve is the imaginary part of $g(x) = x^2 + (ax+b)^2$. We can see the steepest descent path deformation, $L_1 < x_s < L_2$. (a), (b) correspond to cases $x_0 < L_1$, and $L_1 < x_0 < x_s$. (c), (d) correspond to cases $x_s < x_0 < L_2$ and $x_s < x_0 < L_2$.

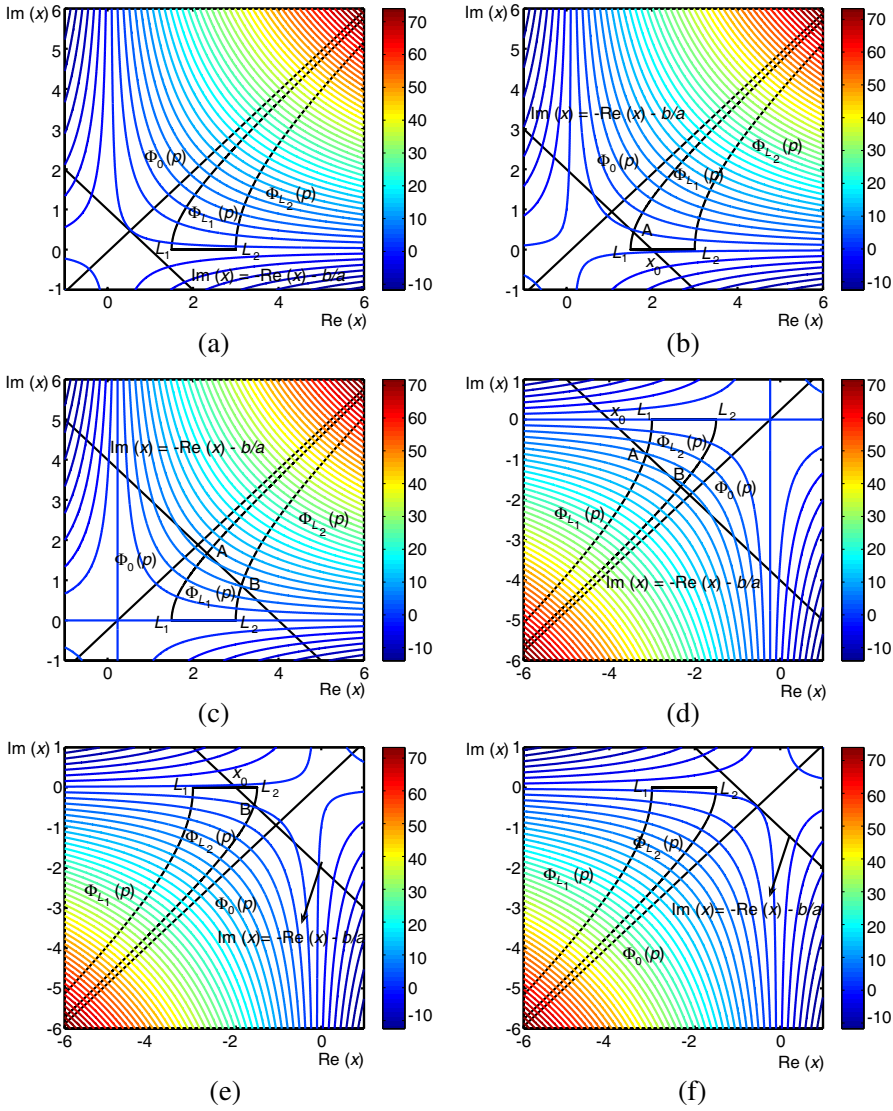

Figure 6. Contour curve is the imaginary part of $g(x) = x^2+(ax+b)^2$. We can see the steepest descent path deformation. (a), (b) correspond to cases $L_1 > x_s$, $x_0 < L_1$ and $L_1 < x_0 < L_2$. (c), (d) correspond to cases $L_1 > x_s$, $L_2 < x_0$ and $L_2 < x_s$, $x_0 < L_1$. (e), (f) correspond to cases $L_2 < x_s$, $L_1 < x_0 < L_2$ and $L_2 < x_0$.

Since the integrand of I_2, i.e., $J_2(x)e^{ikx^2}$ is holomorphic, from Cauchy's integral theorem, its integration value from the two end-points: (L_1, 0) to point (L_2, 0) does not depend on the integral paths we choose. Therefore, we can rewrite I_2 in terms of its steepest descent path form:

$$\begin{aligned} I_2 &= \int_{L_1}^{L_2} J_2^{(a,b)}(x)e^{ikx^2}dx = \int_{\varphi_{\rm SDP}(p)} J_2^{(a,b)}(x)e^{ikx^2}dx \\ &\simeq \underbrace{\int_{\varphi_{\rm SDP}(p)} \left[j_1(x)E^c(x) + j_2^{(a,b)}(x)\right] e^{ik\left(x^2+(ax+b)^2\right)}dx}_{I_2^{\text{non-analytic}}} \\ &\quad + \underbrace{\int_{\varphi_{l_*}} 2j_1(x)e^{ikx^2}dx}_{I_2^{\text{analytic}}}, \end{aligned} \tag{33}$$

where $\varphi_{\rm SDP}(p)$ contains two or three paths of $\varphi_{L_1}(p)$, $\varphi_0(p)$, and $\varphi_{L_2}(p)$ depending on the relative locations of L_1, L_2 and x_s (see Figures 5–6). The integral path φ_{l_*} in Equation (33) comes from the constant term "2" in Equation (24). The integral path φ_{l_*} in Equation (33) comes from the constant term "2" in Equation (24), and is related to the intersection points between the Stokes line $l(ax+b)$ and $\varphi_{\rm SDP}(p)$. All cases for $I_2^{\text{non-analytic}}$ as shown in Figures 5–6 are:

$$I_2^{\text{non-analytic}} = \begin{cases} I_2^1 - I_2^2 + I_2^0, & L_1 < x_s < L_2, \\ I_2^1 - I_2^2, & L_2 < x_s, \text{ or } x_s < L_1. \end{cases} \tag{34}$$

where

$$\begin{aligned} I_2^1 &= \int_{\varphi_{L_1}(p)} \left[j_1(x)E^c(x) + j_2^{(a,b)}(x)\right] e^{ik\left[x^2+(ax+b)^2\right]}dx \\ &= \int_0^\infty e^{-kp}e^{ik\left[L_1^2+(aL_1+b)^2\right]}K_1(p)dp, \end{aligned} \tag{35}$$

$$\begin{aligned} I_2^2 &= \int_{\varphi_{L_2}(p)} \left[j_1(x)E^c(x) + j_2^{(a,b)}(x)\right] e^{ik\left[x^2+(ax+b)^2\right]}dx \\ &= \int_0^\infty e^{-kp}e^{ik\left[L_2^2+(aL_2+b)^2\right]}K_2(p)dp, \end{aligned} \tag{36}$$

$$\begin{aligned} I_2^0 &= \int_{\varphi_0(p)} \left[j_1(x)E^c(x) + j_2^{(a,b)}(x)\right] e^{ik[x^2+(ax+b)^2]}dx \\ &= \int_{-\infty}^\infty e^{-kp^2}e^{ik\left[x_s^2+(ax_s+b)^2\right]}K_0(p)dp, \end{aligned} \tag{37}$$

with

$$K_1(p) = \left[j_1(\varphi_{L_1}(p))E^c(\varphi_{L_1}(p)) + j_2^{(a,b)}(\varphi_{L_1}(p))\right]\varphi'_{L_1}(p),$$

$$K_2(p) = \left[j_1(\varphi_{L_2}(p))E^c(\varphi_{L_2}(p)) + j_2^{(a,b)}(\varphi_{L_2}(p))\right]\varphi'_{L_2}(p),$$

$$K_0(p) = \left[j_1(\varphi_0(p))E^c(\varphi_0(p)) + j_2^{(a,b)}(\varphi_0(p))\right]\varphi'_0(p).$$

The integral I_2^{analytic} has the closed-form expression. The original function of its kernel $2j_1(x)e^{ikx^2}$ is

$$K(x) = \left(-\frac{\pi}{2ik}\alpha_1 - \frac{\pi}{4k^2}\alpha_4 - \frac{\pi}{4k^2}\alpha_5\right)\text{erfc}\left(\sqrt{-ik}x\right) + \left(-\frac{\sqrt{\pi}}{2ik\sqrt{-ik}}\alpha_2 - \frac{\sqrt{\pi}x}{2ik\sqrt{-ik}}\alpha_4\right)e^{ikx^2}. \tag{38}$$

From Figures 5–6, it can be seen that many cases of I_2^{analytic} depend on the relative locations of two end-points $(L_1, 0)$, $(L_2, 0)$, stationary phase point $(x_s, 0) = (-\frac{ab}{1+a^2}, 0)$ and the intersection points of Stokes line with the real x-axis $(x_0, 0) = (-\frac{b}{a}, 0)$. When the slope of line $y = ax + b$ changes from $a > 0$ to $a < 0$ (See Figure 2), domain $\prod$ and $\coprod$ in Equation (25) generated by $\text{erfc}\,(\sqrt{-ik}(ax + b))$ will swap with each other. All possible cases of I_2^{analytic} are given in Appendix B.

Hence, the integral I in Equation (21) can be written as:

$$I = I_2^{\text{non-analytic}} + I_2^{\text{analytic}} - I_1, \tag{39}$$

where $I_2^{\text{non-analytic}}$, I_2^{analytic} and I_1 are given in Equation (34), I_2^{analytic} of Appendix B, and Equation (22), respectively.

3. HIGHLY OSCILLATORY PO INTEGRAL ON THE TRIANGULAR PATCH

In Figure 7(a), we give a triangular patch containing a stationary phase point $\mathbf{X}_s = (0, 0)$ satisfying $\nabla v(\mathbf{X}_s) = [0, 0]^T$, where $v(x, y) = x^2 + y^2$. The three vertex points of the triangular patch are $\mathbf{V}_1 = (L_3, a_1L_3 + b_1) = (L_3, a_3L_3 + b_3)$, $\mathbf{V}_2 = (L_1, a_1L_1 + b_1) = (L_1, a_2L_1 + b_2)$, and $\mathbf{V}_3 = (L_2, a_2L_2 + b_2) = (L_2, a_3L_2 + b_3)$.

To calculate the PO integral on the triangular patch Equation (14), we firstly decompose the triangular patch into two sub-

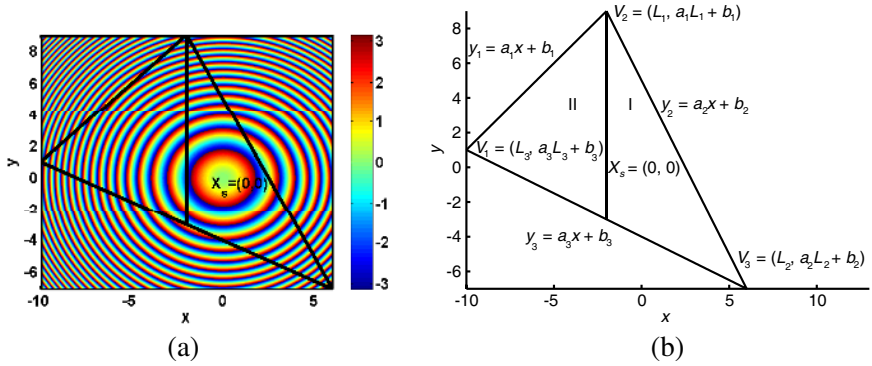

Figure 7. Highly oscillatory integrand $p(x, y)e^{ik(x^2+y^2)}$ on a triangular patch (a). Decomposition of the triangular patch into two parts (b).

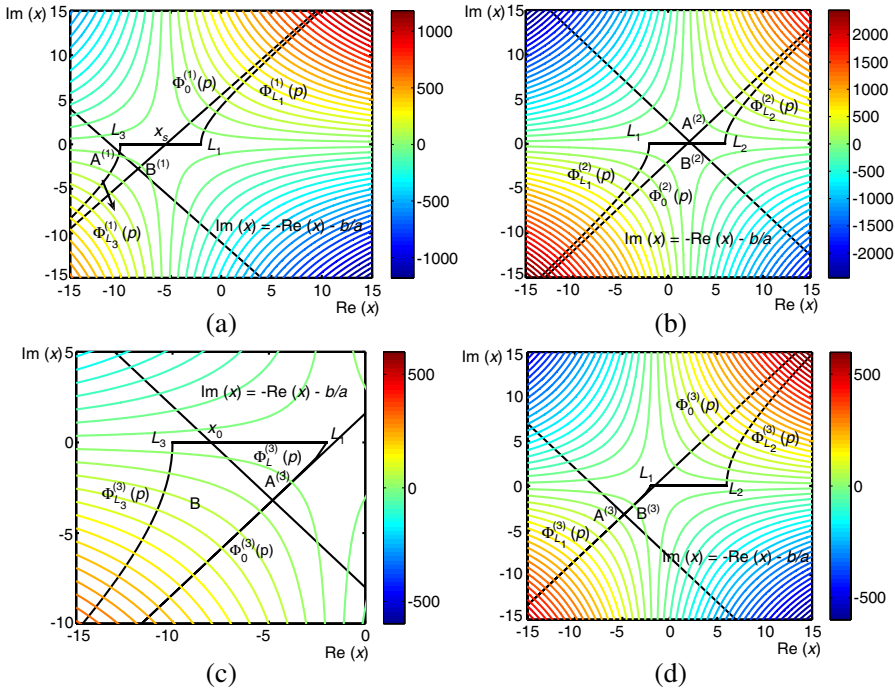

Figure 8. Steepest descent paths for the integrand of I_2 defined on edge 1 (a), edge 2 (b), and edge 3 (c), (d), respectively. The phase functions on the three edges are $g_1(x) = x^2 + (a_1x + b_1)^2$, $g_2(x) = x^2 + (a_2x + b_2)^2$, and $g_3(x) = x^2 + (a_3x + b_3)^2$, respectively.

domains I and II, as shown in Figure 7(b). For domain I, we have

$$\begin{aligned} I^{(\text{right})} &= \int_{L_1}^{L_2} \int_{a_3x+b_3}^{a_2x+b_2} p(x,y) e^{ik(x^2+y^2)} dy dx \\ &= \int_{L_1}^{L_2} J_2^{(a_2,b_2)}(x) e^{ikx^2} dx - \int_{L_1}^{L_2} J_2^{(a_3,b_3)}(x) e^{ikx^2} dx, \end{aligned} \quad (40)$$

where $J_2^{(a_2,b_2)}$ and $J_2^{(a_3,b_3)}$ have the similar forms given in Equation (20):

$$\begin{aligned} J_2^{(a_2,b_2)}(x) &= j_1(x)\text{erfc}\left(\sqrt{-ik}(a_2x+b_2)\right) \\ &\quad + \underbrace{\frac{\alpha_3+\alpha_6x+\alpha_5(a_2x+b_2)}{2ik}}_{j_2^{(a_2,b_2)}(x)} e^{ik(a_2x+b_2)^2}, \end{aligned} \quad (41)$$

$$\begin{aligned} J_2^{(a_3,b_3)}(x) &= j_1(x)\text{erfc}\left(\sqrt{-ik}(a_3x+b_3)\right) \\ &\quad + \underbrace{\frac{\alpha_3+\alpha_6x+\alpha_5(a_3x+b_3)}{2ik}}_{j_2^{(a_3,b_3)}(x)} e^{ik(a_3x+b_3)^2}. \end{aligned} \quad (42)$$

From Figure 8(b), and based on case 3 and $a < 0$ of Appendix B, we have

$$\begin{aligned} &\int_{L_1}^{L_2} J_2^{(a_2,b_2)}(x) e^{ikx^2} dx = \int_{\varphi_{\text{SDP}}^{(a_2,b_2)}} J_2^{(a_2,b_2)}(x) e^{ikx^2} dx \\ &\simeq \int_{\varphi_{\text{SDP}}^{(a_2,b_2)}} \left[j_1(x) E^{c,(a_2,b_2)}(x) + j_2^{(a_2,b_2)}(x) \right] e^{ik\left[x^2+(a_2x+b_2)^2\right]} dx \\ &\quad + \int_{\varphi_{l*}^{(a_2,b_2)}} 2j_1(x) e^{ikx^2} dx \\ &= I_{L_1}^{(a_2,b_2)} + I_{x_s}^{(a_2,b_2)} - I_{L_2}^{(a_2,b_2)} + K((L_2,0)) - K\left(\mathbf{A}^{(2)}\right). \end{aligned} \quad (43)$$

From Figure 8(b), and based on case 1 and $a < 0$ of Appendix B, we have

$$\begin{aligned} &\int_{L_1}^{L_2} J_2^{(a_3,b_3)}(x) e^{ikx^2} dx = \int_{\varphi_{\text{SDP}}^{(a_3,b_3)}} J_2^{(a_3,b_3)}(x) e^{ikx^2} dx \\ &= \int_{\varphi_{\text{SDP}}^{(a_3,b_3)}} \left[j_1(x) E^{c,(a_3,b_3)}(x) + j_2^{(a_3,b_3)}(x) \right] e^{ik\left[x^2+(a_3x+b_3)^2\right]} dx \end{aligned}$$

$$
\begin{aligned}
&+\int_{\varphi_{l_*}^{(a_3,b_3)}} 2j_1(x)e^{ikx^2}dx \\
&= I_{L_1}^{(a_3,b_3)} + I_{x_s}^{(a_3,b_3)} - I_{L_2}^{(a_3,b_3)} + K((L_2,0)) - K\left(\mathbf{B}^{(3)}\right) \\
&+K\left(\mathbf{A}^{(3)}\right) - K((L_1,0)). \qquad (44)
\end{aligned}
$$

Hence, based on Equations (40), (43)–(44), we have

$$
\begin{aligned}
I^{(\text{right})} \;=\; & I_{L_1}^{(a_2,b_2)} + I_{x_s}^{(a_2,b_2)} - I_{L_2}^{(a_2,b_2)} - I_{L_1}^{(a_3,b_3)} - I_{x_s}^{(a_3,b_3)} + I_{L_2}^{(a_3,b_3)} \\
& -K\left(\mathbf{A}^{(2)}\right) + K\left(\mathbf{B}^{(3)}\right) - K\left(\mathbf{A}^{(3)}\right) + K((L_1,0)). \qquad (45)
\end{aligned}
$$

Similarly for domain II, we have

$$
\begin{aligned}
I^{(\text{left})} \;&=\; \int_{L_3}^{L_1}\int_{a_3x+b_3}^{a_1x+b_1} p(x,y)e^{ik(x^2+y^2)}dydx \\
&= \int_{L_3}^{L_1} J_2^{(a_1,b_1)}(x)e^{ikx^2}dx - \int_{L_3}^{L_1} J_2^{(a_3,b_3)}(x)e^{ikx^2}dx, \qquad (46)
\end{aligned}
$$

where $J_2^{(a_1,b_1)}$ has the similar form as $J_2^{(a_3,b_3)}$:

$$
\begin{aligned}
J_2^{(a_1,b_1)}(x) \;=\; & j_1(x)\text{erfc}\left(\sqrt{-ik}(a_1x+b_1)\right) \\
& + \underbrace{\frac{\alpha_3+\alpha_6x+\alpha_5(a_1x+b_1)}{2ik}}_{j_2^{(a_1,b_1)}(x)} e^{ik(a_1x+b_1)^2}. \qquad (47)
\end{aligned}
$$

From Figure 8(a), and based on case 1 and $a > 0$ of Appendix B, we have

$$
\begin{aligned}
&\int_{L_3}^{L_1} J_2^{(a_1,b_1)}(x)e^{ikx^2}dx = \int_{\varphi_{\text{SDP}}^{(a_1,b_1)}} J_2^{(a_1,b_1)}(x)e^{ikx^2}dx \\
&\simeq \int_{\varphi_{\text{SDP}}^{(a_1,b_1)}} \left[j_1(x)E^{c,(a_1,b_1)}(x) + j_2^{(a_1,b_1)}(x)\right] e^{ik\left[x^2+(a_1x+b_1)^2\right]}dx \\
&\quad + \int_{\varphi_{l_*}^{(a_1,b_1)}} 2j_1(x)e^{ikx^2}dx \\
&= I_{L_3}^{(a_1,b_1)} + I_{x_s}^{(a_1,b_1)} - I_{L_1}^{(a_1,b_1)} + K\left(\mathbf{B}^{(1)}\right) - K\left(\mathbf{A}^{(1)}\right). \qquad (48)
\end{aligned}
$$

From Figure 8(b), and based on case 9 and $a < 0$ of Appendix B, we have

$$
\begin{aligned}
\int_{L_3}^{L_1} J_2^{(a_3,b_3)}(x)e^{ikx^2}dx &= \int_{\varphi_{\text{SDP}}^{(a_3,b_3)}} J_2^{(a_3,b_3)}(x)e^{ikx^2}dx, \\
&= I_{L_3}^{(a_3,b_3)} - I_{L_1}^{(a_3,b_3)} + K((L_1,0)) - K\left(\mathbf{A}^{(3)}\right). \qquad (49)
\end{aligned}
$$

Based on Equations (48)–(49), we have

$$\begin{aligned} I^{(\text{left})} &= I_{L_3}^{(a_1,b_1)} + I_{x_s}^{(a_1,b_1)} - I_{L_1}^{(a_1,b_1)} - I_{L_3}^{(a_3,b_3)} + I_{L_1}^{(a_3,b_3)} \\ &\quad + K\left(\mathbf{B}^{(1)}\right) - K\left(\mathbf{A}^{(1)}\right) - K((L_1,0)) + K\left(\mathbf{A}^{(3)}\right), \end{aligned} \tag{50}$$

where

$$\begin{aligned} I_{L_m}^{(a_n,b_n)} &= \int_{\varphi_{L_m}^{(a_n,b_n)}} J_2^{(a_n,b_n)}(x) e^{ikx^2} dx \\ &= \int_0^\infty e^{-kp} e^{ik\left[L_m^2 + (a_n L_m + b_n)^2\right]} H_{mn}(p) dp, \end{aligned} \tag{51}$$

$$\begin{aligned} I_{x_s}^{(a_n,b_n)} &= \int_{\varphi_0^{(a_n,b_n)}} J_2^{(a_n,b_n)}(x) e^{ikx^2} dx \\ &= \int_{-\infty}^\infty e^{-kp^2} e^{ik\left[x_s^2 + (a_n x_s + b_n)^2\right]} T_n(p) dp, \end{aligned} \tag{52}$$

with

$$\begin{aligned} H_{mn}(p) &= \left[j_1\left(\varphi_{L_m}^{(a_n,b_n)}(p)\right) E^c\left(\varphi_{L_m}^{(a_n,b_n)}(p)\right) + j_2^{(a_n,b_n)}\left(\varphi_{L_m}^{(a_n,b_n)}(p)\right)\right] \\ &\quad \cdot \varphi_{L_m}^{(a_n,b_n)'}(p), \\ T_n(p) &= \left[j_1\left(\varphi_0^{(a_n,b_n)}(p)\right) E^c\left(\varphi_0^{(a_n,b_n)}(p)\right) + j_2^{(a_n,b_n)}\left(\varphi_0^{(a_n,b_n)}(p)\right)\right] \\ &\quad \cdot \varphi_0^{(a_n,b_n)'}(p), \quad m,n = 1,2,3. \end{aligned}$$

Above all, based on Equation (45) and Equation (50), we have the closed-form formula for I in Equation (14) on a triangular patch as follows:

$$\begin{aligned} I &= I^{(\text{left})} + I^{(\text{right})} \\ &\simeq \underbrace{I_{L_1}^{(a_2,b_2)} - I_{L_1}^{(a_1,b_1)} + I_{L_2}^{(a_3,b_3)} - I_{L_2}^{(a_2,b_2)} + I_{L_3}^{(a_1,b_1)} - I_{L_3}^{(a_3,b_3)}}_{\text{three vertex point contributions}} \\ &\quad + \underbrace{I_{x_s}^{(a_2,b_2)} - I_{x_s}^{(a_3,b_3)} + I_{x_s}^{(a_1,b_1)}}_{\text{three resonance point contributions}} \\ &\quad + \underbrace{K\left(\mathbf{B}^{(1)}\right) - K\left(\mathbf{A}^{(1)}\right) + K\left(\mathbf{B}^{(3)}\right) - K\left(\mathbf{A}^{(2)}\right)}_{\text{three Stokes lines and numerical SDPs intersection point contributions}} . \end{aligned} \tag{53}$$

The three Stokes lines correspond to Equation (26) on three edges $\text{Im}(x) = -\text{Re}(x) + \frac{b_m}{a_m}$, $m = 1, 2, 3$. The subscript x_s in the "three vertex point contributions" terms $I_{x_s}^{(a_m,b_m)}$, $m = 1, 2, 3$, denotes the

x-component of the three resonance points on the three edges $\overrightarrow{\mathbf{V}_1\mathbf{V}_2}$, $\overrightarrow{\mathbf{V}_2\mathbf{V}_3}$, and $\overrightarrow{\mathbf{V}_3\mathbf{V}_1}$ as shown in Figure 7, respectively.

There is another way to interpret the Equation (53): the PO integral I given in Equation (14) can be decomposed as the summation of $I_2^{(a_m,b_m)}$, $m = 1, 2, 3$, separately. Their formulas are

$$I = I_2^{(a_1,b_1)} + I_2^{(a_2,b_2)} - I_2^{(a_3,b_3)}, \tag{54}$$

where

$$I_2^{(a_1,b_1)} = I_{L_3}^{(a_1,b_1)} + I_{x_s}^{(a_1,b_1)} - I_{L_1}^{(a_1,b_1)} + K\left(\mathbf{B}^{(1)}\right) - K\left(\mathbf{A}^{(1)}\right), \tag{55}$$

$$I_2^{(a_2,b_2)} = I_{L_1}^{(a_2,b_2)} + I_{x_s}^{(a_2,b_2)} - I_{L_2}^{(a_2,b_2)} + K\left((L_2,0)\right) - K\left(\mathbf{A}^{(2)}\right), \tag{56}$$

$$I_2^{(a_3,b_3)} = I_{L_3}^{(a_3,b_3)} + I_{x_s}^{(a_3,b_3)} - I_{L_2}^{(a_3,b_3)} + K\left((L_2,0)\right) - K\left(\mathbf{B}^{(3)}\right). \tag{57}$$

The above Equations (54)–(57) clearly give the decomposition of original PO integral I given in Equation (14) on the triangle three edges. In Section 5, for the numerical examples on the triangular patch, we will use Equations (54)–(57) to calculate our numerical SDP results for the PO integral I.

4. ANALYSIS OF THE CRITICAL POINT CONTRIBUTIONS ON A TRIANGULAR PATCH BY THE NUMERICAL SDP METHOD AND COMPARISON WITH THE TRADITIONAL ASYMPTOTIC APPROXIMATION APPROACH

4.1. Stationary Phase Point Contribution

We again consider the highly oscillatory PO integral defined on the domain I of the triangular patch (see Figure 7), that is, $[L_1, L_2] \times [a_3x + b_3, a_2x + b_2]$, where

$$\tilde{I} = \int_{L_1}^{L_2} \int_{a_3x+b_3}^{a_2x+b_2} p(x,y) e^{ik(x^2+y^2)} dydx. \tag{58}$$

When $L_1 < 0 < L_2$, $a_3x+b_3 \leq 0$ and $a_2x+b_2 \geq 0$, the two dimensional integration domain contains the stationary phase point $\mathbf{X}_s = (0,0)$. We use the asymptotic expansion method [1, 18, 46] for Equation (58) and consider the integral

$$\tilde{I}^1 = \int_{-\infty}^{\infty} \int_{-\infty}^{\infty} p(x,y) e^{ik(x^2+y^2)} dydx. \tag{59}$$

Using integration by parts, the above integral can be derived as follows:

$$\tilde{I}^1 = \int_{-\infty}^{\infty} p_1(x) e^{ikx^2} dx, \tag{60}$$

$$\begin{aligned} p_1(x) &= \int_{-\infty}^{\infty} p(x,y) e^{iky^2} dy \\ &= \left(\alpha_1 + \alpha_2 x + \alpha_4 x^2\right) \Gamma\left(\frac{1}{2}\right) i^{\frac{1}{2}} k^{-\frac{1}{2}} + \alpha_5 \Gamma\left(\frac{3}{2}\right) i^{\frac{3}{2}} k^{-\frac{3}{2}}, \end{aligned} \tag{61}$$

where

$$\int_{-\infty}^{\infty} x^{2n} e^{ikx^2} dx = i^{n+\frac{1}{2}} \Gamma\left(n + \frac{1}{2}\right) k^{-n-\frac{1}{2}},$$

$p_1(x)$ corresponds to the stationary phase point contribution at $y = 0$. Using the above integral identity again into Equation (60), and the fact $\Gamma(\frac{1}{2}) = \sqrt{\pi} = 2\Gamma(\frac{3}{2})$, the stationary phase point contribution term of the integral given in Equation (59) is

$$\tilde{I}^{1,\mathrm{sp}} = -\left(\frac{\pi}{ik}\alpha_1 + \frac{\pi}{2k^2}\alpha_4 + \frac{\pi}{2k^2}\alpha_5\right). \tag{62}$$

It is of $O\left(k^{-1}\right)$.

Now we take a look at the "three Stokes lines and numerical SDPs intersection point contributions" term in Equation (53). We define the following term

$$\begin{aligned} CK &= K\left(\mathbf{B}^{(1)}\right) - K\left(\mathbf{A}^{(1)}\right) + K\left(\mathbf{B}^{(3)}\right) - K\left(\mathbf{A}^{(2)}\right) \\ &= \int_{\mathbf{A}^{(1)}}^{\mathbf{B}^{(1)}} 2j_1(x) e^{ikx^2} dx + \int_{\mathbf{A}^{(2)}}^{\mathbf{B}^{(3)}} 2j_1(x) e^{ikx^2} dx, \end{aligned} \tag{63}$$

where the points $\mathbf{A}^{(1)}$, $\mathbf{B}^{(1)}$, $\mathbf{A}^{(2)}$, $\mathbf{B}^{(3)}$ are the intersection points of Stokes lines and steepest descent paths shown in Figure 8. The second integral term in the right hand of Equation (63) has the integration path from $\mathbf{A}^{(2)}$ to $\mathbf{B}^{(3)}$. It shall contain the stationary phase point in order to form the closed paths. Following the derivation of the stationary phase point contribution in Equation (58), the stationary phase point contribution in Equation (62) can be exactly extracted!

The leading term $(-\frac{\pi}{ik}\alpha_1)$ in Equation (62) agrees well with [13, 18], they are called the "critical points contribution". In this paper, we include the high order terms $(-\frac{\pi}{2k^2}\alpha_4 - \frac{\pi}{2k^2}\alpha_5)$ to gain higher accuracy when k is not large enough (for example $k = 20$).

4.2. Resonance Point Contributions

From Equations (40), (46) and Figure 7, we see that the highly oscillatory integrands defined on the three edges of the triangular

patch are $J_2^{(a_m,b_m)}e^{ikx^2}$, $m = 1, 2, 3$. After the same derivation procedure for the phase behavior of $I_2^{\text{non-analytic}}$ given in Equation (33), the corresponding phase functions of $J_2^{(a_m,b_m)}e^{ikx^2}$ have the formulas $g_m(x, y_m(x)) = x^2 + y_m^2(x)$, and $y_m(x) = a_m x + b_m$, $m = 1, 2, 3$. The phase functions $g_m\left(x, y_m(x)\right)$ may have stationary phase points $x_{r,m}$ satisfying

$$\begin{aligned} & \frac{dg_m(x, y_m(x))}{dx} = \frac{\partial g_m}{\partial x} + \frac{\partial g_m}{\partial y_m}\frac{dy_m(x)}{dx} = 0 \\ \Longleftrightarrow \quad & \nabla g_m \cdot \nabla \begin{bmatrix} x \\ y_m(x) \end{bmatrix} = 0. \end{aligned} \tag{64}$$

After solving $x_{r,m}$ from Equation (64), the resultant three *resonance points* on the three edges of triangular patch as shown in Figure 7 are

$$\mathbf{X}_{r,m} = (x_{r,m}, y_{r,m}) = \left(-\frac{a_m b_m}{1+a_m^2}, \frac{b_m}{1+a_m^2}\right), \quad m = 1, 2, 3, \tag{65}$$

and $y_{r,m} = a_m x_{r,m} + b_m$. Equation (64) shows that $g_m\left(x, y_m(x)\right)$ has stationary points $x_{r,m}$ when the gradient of $g_m\left(x, y_m(x)\right)$ is orthogonal to the tangent line of the boundary parameterized by $[x \quad y_m(x)]^T$ on this point.

Again, we use the asymptotic expansion method [1, 19, 21] to derive the leading terms of resonance point contributions. We consider the integral

$$\tilde{I}^2 = \int_{-\infty}^{\infty}\int_{a_1x+b_1}^{\infty} p(x,y)e^{ik(x^2+y^2)}dydx. \tag{66}$$

Using integration by parts, the above integral can be derived as follows:

$$\begin{aligned} \tilde{I}^2 &= \int_{-\infty}^{\infty}\int_{a_1x+b_1}^{\infty} p(x,y)e^{ik(x^2+y^2)}dydx & (67)\\ &= \int_{-\infty}^{\infty}\int_{a_1x+b_1}^{\infty} p(x,y)e^{iky^2}dye^{ikx^2}dx \\ &\simeq \int_{-\infty}^{\infty} R_1(x)e^{ikx^2}dx, & (68)\\ R_1(x) &= \int_{a_1x+b_1}^{\infty} p(x,y)e^{iky^2}dy \\ &\simeq \sum_{n=0}^{\infty}(i/k)^{1+n}a_n(x)e^{ik(x^2+(a_1x+b_1)^2)}, & (69) \end{aligned}$$

where

$$a_0(x) = \frac{p(x, a_1x+b_1)}{2(a_1x+b_1)}.$$

Following the same procedure as Equation (61), we have the resonance points contribution as follows:

$$\tilde{I}^2 \simeq \sum_{n=0}^{\infty} (1/k)^{3/2+n} b_n e^{ik\left(x_{r,1}^2+y_{r,1}^2\right)}, \tag{70}$$

where the leading term coefficient b_0 has the formula

$$b_0 = \frac{i^{3/2}\sqrt{\pi}p(\mathbf{X}_{r,1})}{2(\mathbf{X}_{r,1}\cdot\hat{\mathbf{n}}_1)\|\hat{\mathbf{t}}_1\|},$$

and $\hat{\mathbf{n}}_1$ and $\hat{\mathbf{t}}_1$ are the normal and tangential vectors of line $y_1(x) = a_1x+b_1$, respectively. The leading term for $\tilde{I}^2$ is $(1/k)^{3/2}b_0e^{ik(x_{r,1}^2+y_{r,1}^2)}$. It is of $O\left(k^{-\frac{3}{2}}\right)$, which is the same as the results in [13, 18]. They called them the boundary critical point contributions. Similarly, for the other two resonance points, we have the similar asymptotic formulas as given in Equation (70).

In this work, the three resonance points contributions by using numerical SDP method are $I_{x_s}^{(a_m,b_m)}$, $m = 1, 2, 3$, defined in Equation (52). Compared with the above asymptotic expansion, less approximation is done by the numerical SDP method. In Section 5, we give the numerical results verification and comparison of $I_{x_s}^{(a_m,b_m)}$ with the leading term of Equation (70).

4.3. Vertex Point Contributions

In Figure 7(b), we denote the intersection points of $y_1 = a_1x + b_1$ and $y_3 = a_3x + b_3$ as $\mathbf{V}_1$. Then we consider the integral

$$\tilde{I}^3 = \int_{-\infty}^{L_3}\int_{-\infty}^{a_3x+b_3} p(x,y)e^{ik(x^2+y^2)}dydx. \tag{71}$$

Using integration by parts, the above integral can be derived as follows:

$$\begin{aligned}
\tilde{I}^3 &= \int_{-\infty}^{L_3}\int_{-\infty}^{a_3x+b_3} p(x,y)e^{ik(x^2+y^2)}dydx. && (72)\\
&= \int_{-\infty}^{L_3}\int_{-\infty}^{a_3x+b_3} p(x,y)e^{iky^2}dye^{ikx^2}dx\\
&\simeq \int_{-\infty}^{L_3} W_1(x)e^{ikx^2}dx, && (73)\\
W_1(x) &\int_{-\infty}^{a_3x+b_3} p(x,y)e^{iky^2}dy\\
&\simeq -\sum_{n=0}^{\infty}(i/k)^{1+n}d_n(x)e^{ik\left(x^2+(a_3x+b_3)^2\right)}, && (74)
\end{aligned}$$

where

$$d_0(x) = \frac{p(x, a_3x + b_3)}{2(a_3x + b_3)}.$$

Doing the same procedure for the Equation (74), we have the vertex point contribution as follows:

$$\tilde{I}^3 \simeq -\sum_{n=0}^{\infty}(1/k)^{2+n}c_n e^{ik\left[L_3^2+(a_3L_3+b_3)^2\right]}, \tag{75}$$

where

$$c_0 = \frac{|\hat{\mathbf{t}}_1 \times \hat{\mathbf{t}}_3|p(\mathbf{V}_1)}{2\mathbf{V}_1 \cdot (\hat{\mathbf{t}}_1 + \hat{\mathbf{t}}_3)}.$$

Thus the leading term for Equation (75) is of $O\left(k^{-2}\right)$, which is the same as [13]. In this work, the three vertex point contributions calculated by using the numerical SDP method are

$$I_{\mathbf{V}_1} = I_{L_3}^{(a_1,b_1)} - I_{L_3}^{(a_3,b_3)} \quad \text{for vertex}\,\mathbf{V}_1. \tag{76}$$

$$I_{\mathbf{V}_2} = I_{L_1}^{(a_2,b_2)} - I_{L_1}^{(a_1,b_1)} \quad \text{for vertex}\,\mathbf{V}_2, \tag{77}$$

$$I_{\mathbf{V}_3} = I_{L_2}^{(a_3,b_3)} - I_{L_2}^{(a_2,b_2)} \quad \text{for vertex}\,\mathbf{V}_3. \tag{78}$$

From Equations (62), (70) and (75), we can see that the stationary phase point, resonance point and vertex point contributions are of $O\left(k^{-1}\right)$, $O\left(k^{-\frac{3}{2}}\right)$, $O\left(k^{-2}\right)$, respectively. Hence, when $k \to \infty$, the stationary phase point contribution becomes the dominant term for the PO integral, which agrees well with geometrical optics (GO) [2, 19, 22]. Previous work [13] only gives the leading term of $O\left(k^{-1}\right)$. But our derivation provides the higher order term using numerical SDP method and achieves higher accuracy that will be demonstrated in Section 5.

4.4. Cancellation of the Resonance and Vertex Points Contributions

Physically, the contributions for the PO integral I given in Equation (4) come from the stationary phase point, the boundary resonance points and boundary vertex points. For practical engineering models, when we assemble discretized triangles together, the internal resonance and vertex point contributions shall cancel each other.

Proposition 1 (Cancellation of the internal resonance point contributions). *Every internal resonance point contribution to the PO integral I by the numerical SDP method is* 0.

Proof. Firstly, from Figure 9, we can see that $\Delta_{\mathbf{V}_1\mathbf{V}_2\mathbf{V}_3}$ contains three resonance points $\mathbf{X}_{r,m}$, $m = 1, 2, 3$. The closed-form PO integral formula I for the triangular patch $\Delta_{\mathbf{V}_1\mathbf{V}_2\mathbf{V}_3}$ is derived in Equation (54).

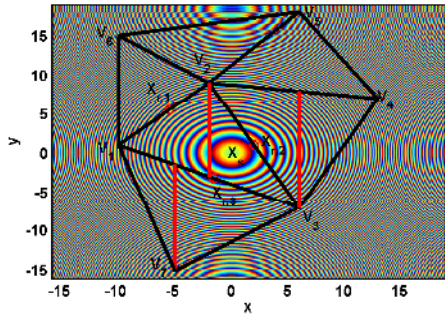

Figure 9. Diagram of a group of assembled triangles containing a stationary phase point $\mathbf{X}_s$, an internal vertex point $\mathbf{V}_2$ and some internal resonance points $\mathbf{X}_{r,m}$, $m = 1, 2, 3$.

Secondly, we analyze the resonance points $\mathbf{X}_{r,m}$ one by one, $m = 1, 2, 3$. For the resonance point $\mathbf{X}_{r,2}$ lying on edge $\mathbf{V}_2\mathbf{V}_3$, it is shared by two triangular patches $\Delta_{\mathbf{V}_1\mathbf{V}_2\mathbf{V}_3}$ and $\Delta_{\mathbf{V}_2\mathbf{V}_4\mathbf{V}_3}$. The resonance point $\mathbf{X}_{r,2}$'s contribution on $\Delta_{\mathbf{V}_1\mathbf{V}_2\mathbf{V}_3}$ is $I_{x_s}^{(a_2,b_2)}$ as given in Equation (54). For simplification, it is re-denoted as $I_{x_s}^{(\mathbf{V}_2,\mathbf{V}_3)}$, where the subscript $x_s = x_{r,2}$ denotes the x-component of the resonance point $\mathbf{X}_{r,2}$ expressed in Equation (65) on the edge $\overrightarrow{\mathbf{V}_2\mathbf{V}_3}$.

Following the numerical SDP closed-form derivation on the triangular patch $\Delta_{\mathbf{V}_1\mathbf{V}_2\mathbf{V}_3}$, for the $\Delta_{\mathbf{V}_2\mathbf{V}_4\mathbf{V}_3}$, we have

$$\begin{aligned} & I_{\Delta_{\mathbf{V}_2\mathbf{V}_4\mathbf{V}_3}} \\ = \; & I^{(\text{left})}_{\Delta_{\mathbf{V}_2\mathbf{V}_4\mathbf{V}_3}} + I^{(\text{right})}_{\Delta_{\mathbf{V}_2\mathbf{V}_4\mathbf{V}_3}} \\ \simeq \; & \underbrace{I_{\mathbf{V}_2}^{(\mathbf{V}_2,\mathbf{V}_4)} - I_{\mathbf{V}_2}^{(\mathbf{V}_2,\mathbf{V}_3)} + I_{\mathbf{V}_4}^{(\mathbf{V}_3,\mathbf{V}_4)} - I_{\mathbf{V}_4}^{(\mathbf{V}_2,\mathbf{V}_4)} + I_{\mathbf{V}_3}^{(\mathbf{V}_2,\mathbf{V}_3)} - I_{\mathbf{V}_3}^{(\mathbf{V}_3,\mathbf{V}_4)}}_{\text{three vertex point contributions}} \\ & \underbrace{-I_{x_s}^{(\mathbf{V}_2,\mathbf{V}_3)} + I_{x_s}^{(\mathbf{V}_2,\mathbf{V}_4)} H(\mathbf{X}_s,\mathbf{V}_2,\mathbf{V}_4) + I_{x_s}^{(\mathbf{V}_3,\mathbf{V}_4)} H(\mathbf{X}_s,\mathbf{V}_3,\mathbf{V}_4)}_{\text{three resonance point contributions}}. \end{aligned} \tag{79}$$

For the notation simplification, $I_{\mathbf{V}_2}^{(\mathbf{V}_2,\mathbf{V}_3)}$ in Equation (79) denotes the vertex point $\mathbf{V}_2$'s contribution on the edge $\overrightarrow{\mathbf{V}_2\mathbf{V}_3}$, it corresponds to the $I_{L_2}^{(a_2,b_2)}$ term in Equation (54). Other terms $I_{\mathbf{V}_j}^{(\mathbf{V}_m,\mathbf{V}_n)}$ in Equation (79) have the similar meanings, m, n, $j = 2, 3, 4$. $H(\mathbf{X}_s,\mathbf{V}_2,\mathbf{V}_4)$ and $H(\mathbf{X}_s,\mathbf{V}_3,\mathbf{V}_4)$ given in Equation (79) are two special functions. When the resonance point in Equation (65) exists between vertex points $\mathbf{V}_2$ and $\mathbf{V}_4$, $H(\mathbf{X}_s,\mathbf{V}_2,\mathbf{V}_4) = 1$, otherwise, $H(\mathbf{X}_s,\mathbf{V}_2,\mathbf{V}_4) = 0$. Similar

argument holds for $H(\mathbf{X}_s, \mathbf{V}_3, \mathbf{V}_4)$.

The resonance point $\mathbf{X}_{r,2}$'s contribution on $\Delta_{\mathbf{V}_2\mathbf{V}_4\mathbf{V}_3}$ is $-I_{x_s}^{(\mathbf{V}_2,\mathbf{V}_3)}$ given in Equation (79), which cancels $\mathbf{X}_{r,2}$'s contribution $I_{x_s}^{(\mathbf{V}_2,\mathbf{V}_3)}$ on $\Delta_{\mathbf{V}_1\mathbf{V}_2\mathbf{V}_3}$. For the other two resonance points $\mathbf{X}_{r,1}$ and $\mathbf{X}_{r,3}$, they are shared by the triangular patches groups $\{\Delta_{\mathbf{V}_1\mathbf{V}_2\mathbf{V}_3}, \Delta_{\mathbf{V}_1\mathbf{V}_6\mathbf{V}_2}\}$ and $\{\Delta_{\mathbf{V}_1\mathbf{V}_2\mathbf{V}_3}, \Delta_{\mathbf{V}_1\mathbf{V}_3\mathbf{V}_7}\}$. Based on the above derivation, the total resonance point $\mathbf{X}_{r,m}$'s contributions are all 0, $m = 1, 2, 3$. Since every internal resonance point is shared by two triangular patches, following the above argument, we conclude that every internal resonance point contribution by using the numerical SDP method are 0. This fact completes the proof.

Remark 1. Because $\Delta_{\mathbf{V}_2\mathbf{V}_4\mathbf{V}_3}$ does not contain the stationary phase point, the stationary phase point contribution does not exist in Equation (79).

Remark 2. Every boundary resonance point is not shared by two triangles. Hence, the boundary resonance point contribution shall exist from the argument in Proposition 1.

Proposition 2 (Cancellation of the internal vertex point contributions). *Every internal vertex point contribution to the PO integral I by the numerical SDP method is* 0.

Proof. Firstly, from Figure 9, the internal vertex point $\mathbf{V}_2$ is shared by five triangular patches: $\Delta_{\mathbf{V}_1\mathbf{V}_2\mathbf{V}_3}$, $\Delta_{\mathbf{V}_2\mathbf{V}_4\mathbf{V}_3}$, $\Delta_{\mathbf{V}_2\mathbf{V}_5\mathbf{V}_4}$, $\Delta_{\mathbf{V}_6\mathbf{V}_5\mathbf{V}_2}$ and $\Delta_{\mathbf{V}_6\mathbf{V}_1\mathbf{V}_2}$. From Equation (54), the vertex point $\mathbf{V}_2$'s contribution on $\Delta_{\mathbf{V}_1\mathbf{V}_2\mathbf{V}_3}$ is

$$I_{\mathbf{V}_2,\,\Delta_{\mathbf{V}_1\mathbf{V}_2\mathbf{V}_3}} = I_{L_1}^{(a_2,b_2)} - I_{L_1}^{(a_1,b_1)} \triangleq I_{\mathbf{V}_2}^{(\mathbf{V}_2,\mathbf{V}_3)} - I_{\mathbf{V}_2}^{(\mathbf{V}_1,\mathbf{V}_2)}. \tag{80}$$

From Equation (79), the vertex point $\mathbf{V}_2$'s contribution on $\Delta_{\mathbf{V}_2\mathbf{V}_4\mathbf{V}_3}$ is

$$I_{\mathbf{V}_2,\,\Delta_{\mathbf{V}_2\mathbf{V}_4\mathbf{V}_3}} = I_{\mathbf{V}_2}^{(\mathbf{V}_2,\mathbf{V}_4)} - I_{\mathbf{V}_2}^{(\mathbf{V}_2,\mathbf{V}_3)}. \tag{81}$$

Secondly, following the derivation of PO integral I's closed-form formula on the other three triangular patches, we have

$$I_{\mathbf{V}_2,\,\Delta_{\mathbf{V}_2\mathbf{V}_5\mathbf{V}_4}} = I_{\mathbf{V}_2}^{(\mathbf{V}_2,\mathbf{V}_5)} - I_{\mathbf{V}_2}^{(\mathbf{V}_2,\mathbf{V}_4)}, \tag{82}$$

$$I_{\mathbf{V}_2,\,\Delta_{\mathbf{V}_6\mathbf{V}_5\mathbf{V}_2}} = I_{\mathbf{V}_2}^{(\mathbf{V}_2,\mathbf{V}_6)} - I_{\mathbf{V}_2}^{(\mathbf{V}_2,\mathbf{V}_5)}, \tag{83}$$

$$I_{\mathbf{V}_2,\,\Delta_{\mathbf{V}_1\mathbf{V}_6\mathbf{V}_2}} = I_{\mathbf{V}_2}^{(\mathbf{V}_1,\mathbf{V}_2)} - I_{\mathbf{V}_2}^{(\mathbf{V}_2,\mathbf{V}_6)}. \tag{84}$$

Summing the above five equations, we get the internal vertex point $\mathbf{V}_2$'s contribution $I_{\mathbf{V}_2}$ to the PO integral I is 0.

Because every internal vertex point is shared by a finite number of edges, and each edge is shared by two triangular patches, the contributions appeared on these two triangular patches cancel each

other. After considering all the edges passing through the internal vertex point, we conclude that every internal vertex point contribution by the numerical SDP method is 0. This fact completes the proof.

Remark 3. For the boundary vertex point, there always exists one edge passing through this vertex point, and this edge is not shared by two triangles. The considered vertex point contribution for the PO integral I on this triangle cannot be canceled. Hence, the boundary vertex point contribution shall exist from the argument in Proposition 2.

5. NUMERICAL EXAMPLES

The following numerical results illustrate that when k is not large enough such as k is around 50, our numerical SDP method can significantly improve the accuracy by one to two digits (10^{-1} to 10^{-2}) compared with the asymptotic approximation approach. When $k \to \infty$, both methods shall and do agree quite well.

5.1. The Right-angled Trapezoid Domains Examples

The first numerical example is a highly oscillatory integral I_2 defined in Equation (33). We can see the integrals I_2^1, I_2^2, and I_2^0 in these three integration formulas in Equations (35)–(38) have the exponentially decay terms e^{-kp} and e^{-kp^2}, respectively. Gauss-Legendre numerical integration schemes [47] are used to calculate these integrals on steepest descent paths. The integration regions for the steepest descent path parameter p are $[0,\ p_1]$ for Equations (35)–(37), and $[-p_2,\ p_2]$ for Equation (38), respectively. The exponentially decay terms e^{-kp} for the integrands of I_2^1, I_2^2, and e^{-kp^2} for I_2^0 as shown in Equations (35)–(38) are constant with $kp_1 = kp_2^2 \equiv 12$. The number of integration points for the Gauss-Legendre numerical integration scheme is fixed to $N = 20$. Therefore, the computational efforts of numerical SDP derived formulas Equations (35)–(38) combined with the Gauss-Legendre numerical integration scheme are k-independent.

The target integral I_2 as shown in Equation (33) has the following setups: endpoints $L_1 = -0.5$, and $L_2 = 0.5$. Trapezoid line is $y = 0.25x - 0.25$. Amplitude function $p(x, y)$'s coefficients as shown in Equation (15) are $\alpha_1 = 0.9501$, $\alpha_2 = 0.2311$, $\alpha_3 = 0.6068$, $\alpha_4 = 0.4860$, $\alpha_5 = 0.8913$, $\alpha_6 = 0.7621$ in integral I_2. The steepest descent paths correspond to Figure 5(d). Numerical results for I_2 by the numerical SDP formulas, Equations (35)–(38) are compared with the results of the direct Matlab quad( ) function in Table 1. We can see when $k \leq 500$, the results by the two methods agree quite well. However,

Table 1. Comparison of integral I_2 (Equation (33)) by using our SDP formulas Equations (35)–(38) and Matlab quad( ) function.

k	Matlab quad( )	SDP method
1	$-0.4675 - 1.2514i$	$-0.4675 - 1.2514i$
10	$-0.0520 - 0.3606i$	$-0.0520 - 0.3606i$
100	$-0.0028 - 0.0234i$	$-0.0028 - 0.0234i$
500	$0.0003 - 0.0055i$	$0.0003 - 0.0055i$
800	$-0.0038 + 0.0041i$	$0.0001 - 0.0037i$
1000	$0.0003 - 0.0049i$	$0.0001 - 0.0030i$

Table 2. Comparison of integral I_2 (Equation (33)) by using our numerical SDP formulas Equations (35)–(38) and brute force method. Other parameters are the same as Table 1.

k	$N(k)$	Brute force	SDP method
1	1	$-0.4675 - 1.2514i$	$-0.4675 - 1.2514i$
10	1	$-0.0520 - 0.3606i$	$-0.0520 - 0.3606i$
100	1	$-0.0028 - 0.0234i$	$-0.0028 - 0.0234i$
500	1	$0.0003 - 0.0055i$	$0.0003 - 0.0055i$
800	11	$0.0001 - 0.0037i$	$0.0001 - 0.0037i$
1000	20	$0.0001 - 0.0030i$	$0.0001 - 0.0030i$

Table 3. Comparison of integral I_2 (Equation (33)) by using our numerical SDP formulas Equations (35)–(38)) and brute force method. Other parameters are the same as Table 1 except for changing $L_1 = 0.5$, $L_2 = 0.75$.

k	$N(k)$	Brute force	numerical SDP method
1	1	$0.0103 - 0.4354i$	$0.0103 - 0.4354i$
10	1	$0.0029 + 0.0750i$	$0.0029 + 0.0750i$
100	25	7.9728e-4 $- 7.6898e\text{-}4i$	7.9728e-4 $- 7.6898e\text{-}4i$
500	50	1.3149e-4 $- 8.0834e\text{-}5i$	1.3149e-4 $- 8.0833e\text{-}5i$
800	100	5.3560e-5 $- 7.9188e\text{-}5i$	5.3560e-5 $- 7.9188e\text{-}5i$
1000	150	1.3219e-5 $- 8.7249e\text{-}5i$	1.3219e-5 $- 8.7249e\text{-}5i$

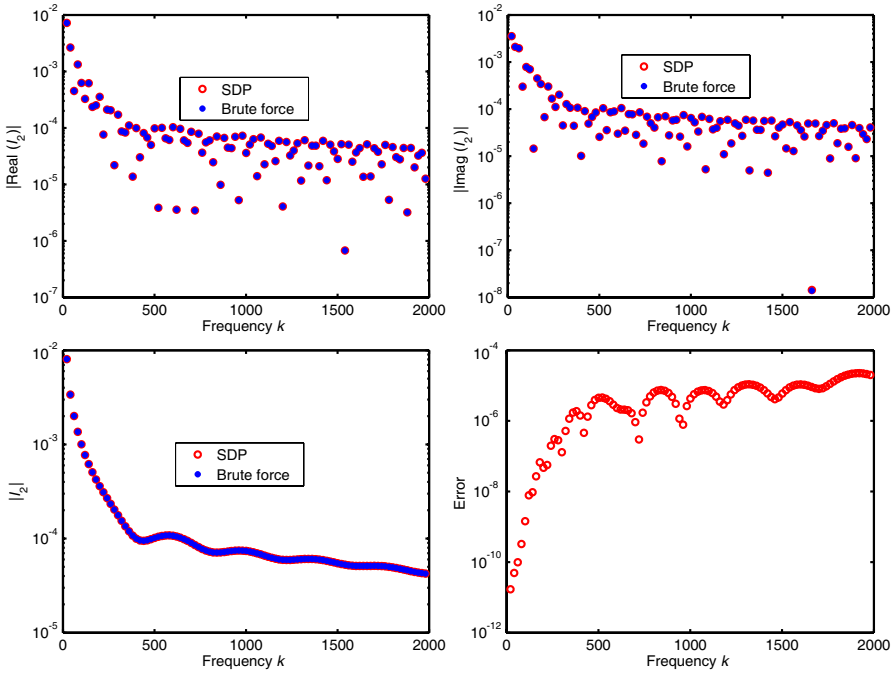

Figure 10. The parameters are the same as Table 2. Comparison of the I_2 integral results by using the numerical SDP and the brute force methods, where we set $N(k) = \lceil k/2 \rceil$ (the upper integer of $k/2$).

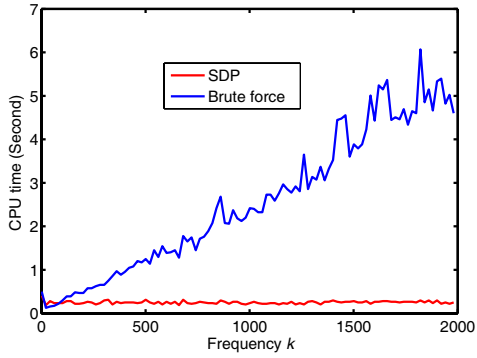

Figure 11. Comparison CPU time for calculating the I_2 integral as shown in Figure 10 by using the numerical SDP and the brute force methods.

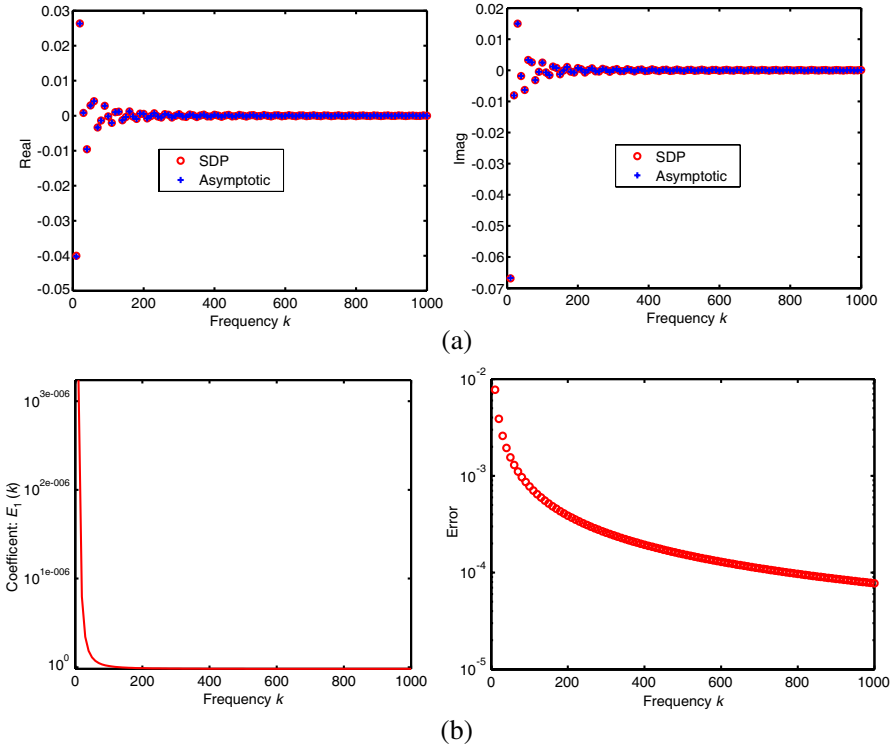

Figure 12. Edge 1: Comparison of the real and imaginary parts of the numerical SDP closed-form formula $I_{x_s}^{(a_1,b_1)}$ results (Equation (55)) by using the asymptotic approximation with leading term $b_0 e^{ik(x_{r,1}^2+y_{r,1}^2)}/k^{3/2}$ [18] (a). $E_1(k) = |R_1(k)/b_0|$, where the coefficients $R_1(k) = I_{\mathbf{X}_s}^{(a_1,b_1)} k^{3/2}$ and $b_0 = -1.7423 + 1.7423i$. Error $= |R_1(k) - b_0 e^{ik(x_{r,1}^2+y_{r,1}^2)}|$ (b).

when $k > 500$, the results begin to have significant differences. The reason is that the I_2 integral becomes highly oscillatory when frequency k goes higher, as shown in Figure 1. As a result, the direct Matlab quad( ) loses the accuracy. In this sense, we divide domain $[L_1, L_2]$ into $N(k)$ small sub-domains $[d_m, d_{m+1}]$, with $d_1 = L_1$ and $d_{N(k)+1} = L_2$, such that

$$[L_1, L_2] = \bigcup_{m=1}^{N(k)} [d_m, d_{m+1}],$$

and Matlab quad( ) function is used in each sub-domain $[d_m, d_{m+1}]$.

This is the brute force method employed for verification in this paper. We can see that the results by these two methods agree well now in Table 2. However, $N(k)$ grows linearly with increasing k. Hence, the computational cost by using the brute force method grows linearly.

To see the different relative locations of the two end-points, and the stationary phase points, we reset $L_1 = 0.5$, $L_2 = 0.75$, which corresponds to in Figure 6(c). Other parameters are the same as Table 1. The resultant integral I_2 numerical results are given in Table 3. Again, the results agree quite well by the brute force and the numerical SDP methods.

Figures 10–11 depict that the I_2 results and CPU time consumed comparison by the numerical SDP and the brute force methods. It can be seen that using the numerical SDP method for calculating I_2 on an arbitrary line is frequency-independent in computational effort and error-controllable in accuracy.

5.2. The Triangular Patch Example

The second numerical example is to compute the highly oscillatory PO integral I in Equation (14) defined on the triangular patch as shown in Figure 7. The three edge equations on the triangular patch are: $l_1 : y = a_1x + b_1 = x + 11$, $l_2 : y = a_2x + b_2 = -2x + 5$, and $l_3 : y = a_3x + b_3 = -0.5x - 4$. The three vertex points are $\mathbf{V}_1 = (-10, 1)$, $\mathbf{V}_2 = (-2, 9)$, and $\mathbf{V}_3 = (6, -7)$. The size of the triangular patch is $L = 17.8885$. It should be noted that when $kL \gg 1$, the PO integral method is accurate to capture the characteristic of the far field. Table 4 shows that the integral I results on a triangular patch by using the numerical SDP method agree very well with the brute force method — sub-dividing Matlab quad( ) function for the highly oscillatory PO integral I. In this sense, using the numerical SDP method for calculating PO integral I is error-controllable.

Table 4. On the triangular patch, the highly oscillatory PO integral I by using the numerical SDP closed-form formula Equation (54) and the brute force method.

k	$N(k)$	Brute force	numerical SDP results
10	1	$0.0611 + 0.3951i$	$0.0611 + 0.3951i$
50	1200	$-0.0082 + 0.0509i$	$-0.0082 + 0.0509i$
100	12000	$-0.0051 + 0.0264i$	$-0.0051 + 0.0264i$
500	60000	$-0.3550\text{e-}3 + 0.6004\text{e-}2i$	$-0.3518\text{e-}3 + 0.6006\text{e-}2i$
1000	120000	$0.4754\text{e-}4 + 0.2868\text{e-}2i$	$0.4219\text{e-}4 + 0.2877\text{e-}2i$

5.3. Comparisons of the Numerical SDP Results with Traditional Asymptotic Approximations on the Triangular Patch

5.3.1. The Resonance Point Contribution Results (Figures 12–14)

The three resonance points on the triangular patch as shown in Figure 7 are given in Equation (65). Pathak [18] and Borovikov [21] gave the asymptotic approximation leading terms for resonance points. From Equation (36) in [18], or Equation (70), we have the leading coefficients $b_0 = -1.7423 + 1.7423i$, $-1.7876 + 1.7876i$, and $2.2615 - 2.2615i$,

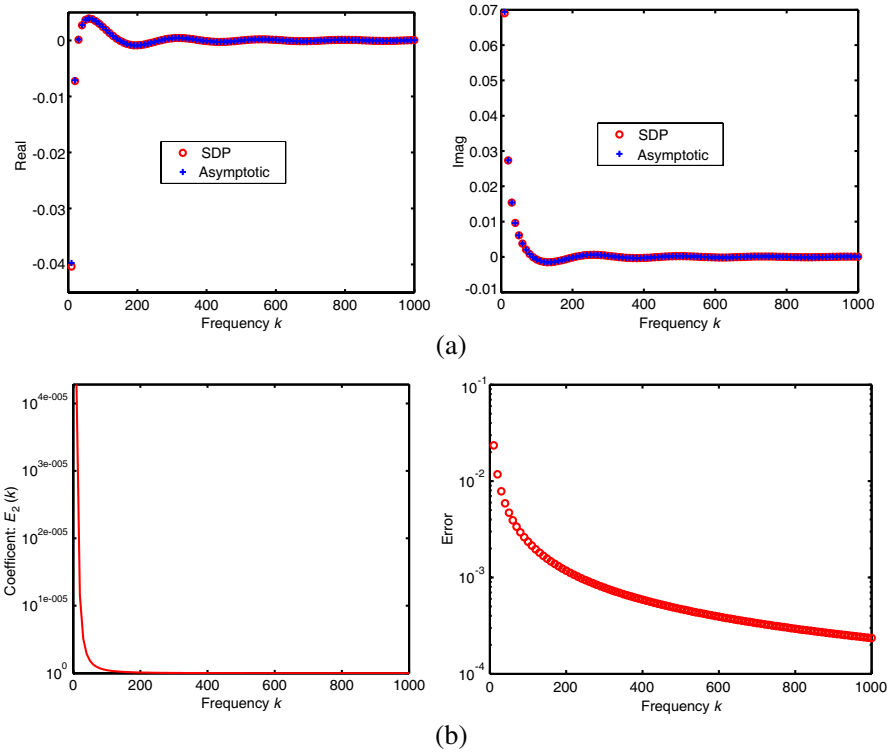

Figure 13. Edge 2: Comparison of the real and imaginary parts of the numerical SDP closed-form formula $I_{x_s}^{(a_2,b_2)}$ results (Equation (56)) by using the asymptotic approximation with leading term $b_0 e^{ik(x_{r,2}^2+y_{r,2}^2)}/k^{3/2}$ [18] (a). $E_2(k) = |R_2(k)/b_0|$, where the coefficients $R_2(k) = I_{\mathbf{X}_s}^{(a_2,b_2)} k^{3/2}$ and $b_0 = -1.7876 + 1.7876i$. Error $= |R_2(k) - b_0 e^{ik(x_{r,2}^2+y_{r,2}^2)}|$ (b).

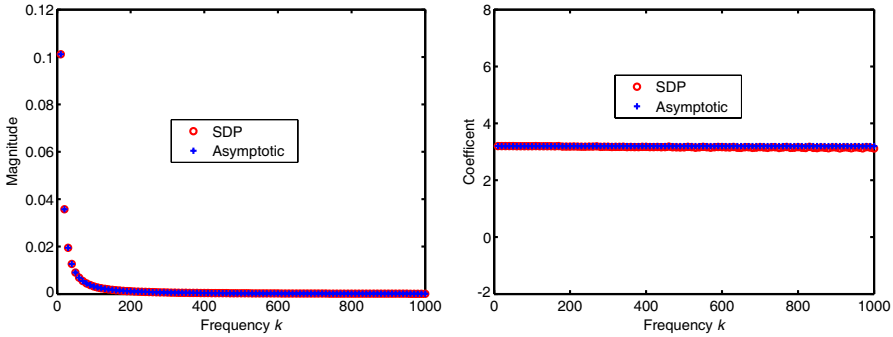

Figure 14. Edge 3: Comparison of the magnitudes of the numerical SDP closed-form formula $|I_{x_s}^{(a_3,b_3)}|$ results (Equation (57)) by using the asymptotic approximation with leading term $|b_0 e^{ik(x_{r,3}^2+y_{r,3}^2)}/k^{3/2}|$ [18] (a). Comparison of the coefficients $|R_3(k)| = |I_{\mathbf{X}_s}^{(a_3,b_3)} k^{3/2}|$ and $|b_0| = |b_0 e^{ik(x_{r,3}^2+y_{r,3}^2)}|$ (b).

and $|b_0| = 2.4640$, 2.5280, and 3.1983 for edge 1, edge 2 and edge 3, respectively.

Figures 12–14 depict the general agreement of the three resonance point contribution results by using the numerical SDP and asymptotic approximation methods on the triangular patch. Furthermore, we introduce $|R_m(k)| = |I_{x_s}^{(a_m,b_m)} k^{3/2}|$, $m = 1, 2, 3$. From Figures 12(b)–14(b), the numerical SDP closed-form formulas $I_{x_s}^{(a_m,b_m)}$ given in Equations (55)–(57) are of $O(k^{-3/2})$, $m = 1, 2, 3$.

5.3.2. Vertex Point Contribution Results (Figures 15–17)

Pathak [18] and Borovikov [21] also gave the asymptotic expansion approximation leading terms for the vertex points. From Equation (37) in [18] or Equation (75), we have the leading vertex point coefficients $c_0 = 0.1632$, -0.3556, and 0.0538, for vertex points $\mathbf{V}_1$, $\mathbf{V}_2$, and $\mathbf{V}_3$, respectively.

Figures 15–17 show the general agreement of the three vertex point contribution results by using the numerical SDP and asymptotic approximation methods on the triangular patch. Furthermore, we introduce $|T_m(k)| = |I_{\mathbf{V}_m} k^2|$, $m = 1, 2, 3$. From Figures 15–17, the numerical SDP closed-form formulas $I_{\mathbf{V}_m}$ given in Equations (76)–(78) are of $O(k^{-2})$.

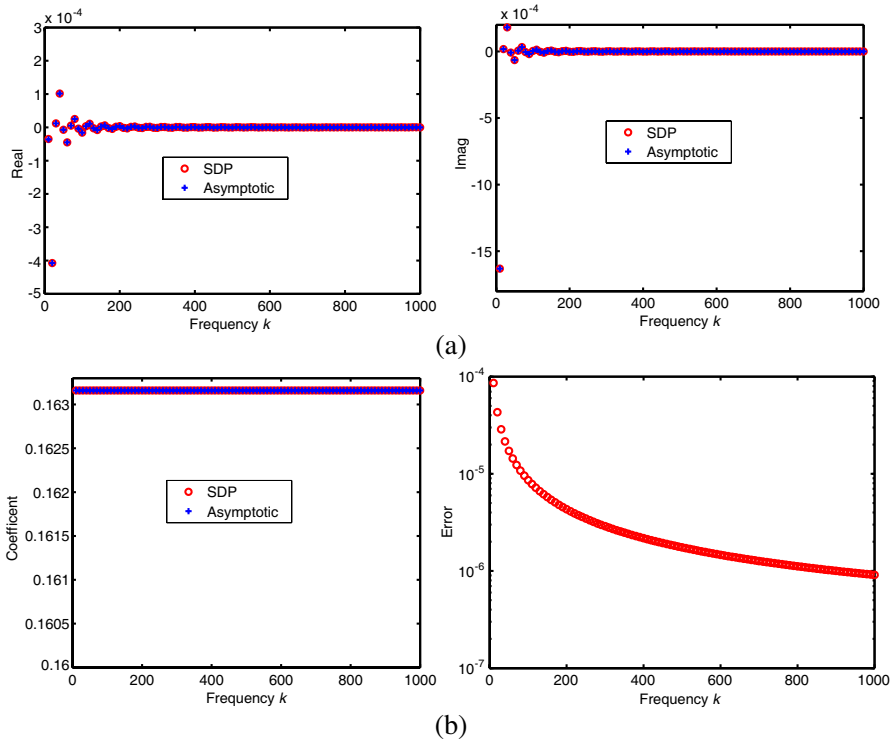

Figure 15. Vertex point V_1: Comparison of the real and imaginary parts of the numerical SDP closed-form formula $I_{\mathbf{V}_1} = I_{L_3}^{(a_1,b_1)} - I_{L_3}^{(a_3,b_3)}$ results (Equations (55)–(57)) by using the asymptotic approximation with leading term $c_0 e^{ik[L_3^2+(a_3L_3+b_3)^2]}/k^2$ [18] (a). Comparison of the coefficients $T_1(k) = |I_{\mathbf{V}_1} \times k^2|$ and $|c_0| = |c_0 e^{ik[L_3^2+(a_3L_3+b_3)^2]}|$. Error $= |T_1(k) - c_0 e^{ik[L_3^2+(a_3L_3+b_3)^2]}|$ (b).

5.3.3. Stationary Phase Point Contribution Results (Figure 18)

In the asymptotic expansion approximation [18], the leading stationary phase point contribution term is $J_s = -\frac{\pi}{ik}\alpha_1$. However, it omits the higher order $O\left(k^{-2}\right)$ terms $-\frac{\pi}{2k^2}\alpha_4 - \frac{\pi}{2k^2}\alpha_5$.

We use three ways to compare the stationary phase point contribution results in Figure 18: Equation (35) in [18], the derived formula Equation (62) by using asymptotic approximation and the numerical SDP method

$$CK = K\left(\mathbf{B}^{(1)}\right) - K\left(\mathbf{A}^{(1)}\right) + K\left(\mathbf{B}^{(3)}\right) - K\left(\mathbf{A}^{(2)}\right) \qquad (85)$$

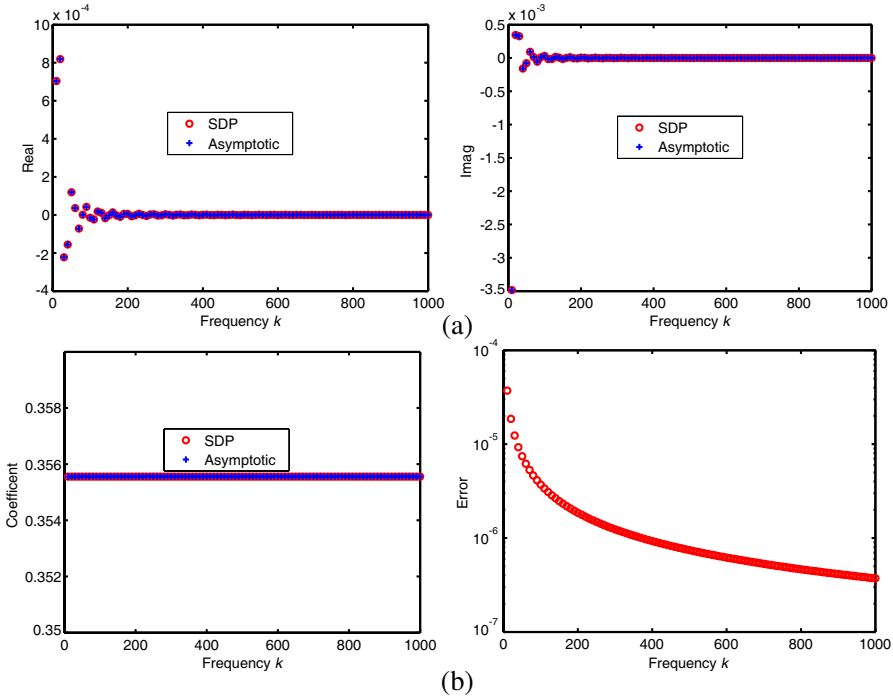

Figure 16. Vertex point $\mathbf{V}_2$: Comparison of the real and imaginary parts of the numerical SDP closed-form formula $I_{\mathbf{V}_2} = I_{L_1}^{(a_2,b_2)} - I_{L_1}^{(a_1,b_1)}$ results (Equations (55)–(56)) by using the asymptotic approximation with leading term $c_0 e^{ik[L_1^2+(a_1L_1+b_1)^2]}/k^2$ [18] (a). Comparison of the coefficients $T_2(k) = |I_{\mathbf{V}_2} \times k^2|$ and $|c_0| = |c_0 e^{ik[L_1^2+(a_1L_1+b_1)^2]}|$. Error $= |T_2(k) - c_0 e^{ik[L_1^2+(a_1L_1+b_1)^2]}|$ (b).

given in Equation (53). Figure 18 presents that when k goes higher, the results obtained by the numerical SDP method and asymptotic approximation in [18] agree very well. Moreover, when k is around 50, the numerical SDP method improves the accuracy by two digits (10^{-2}) by the confirmation of closed-form formula Equation (62) as shown in Figure 18(b).

5.3.4. Total Contribution Points Results (Figures 19–21)

Summarizing the above resonance point, vertex point and the stationary phase point contributions, we give the comparison of highly oscillatory integral I given in Equation (14) on the triangular patch in

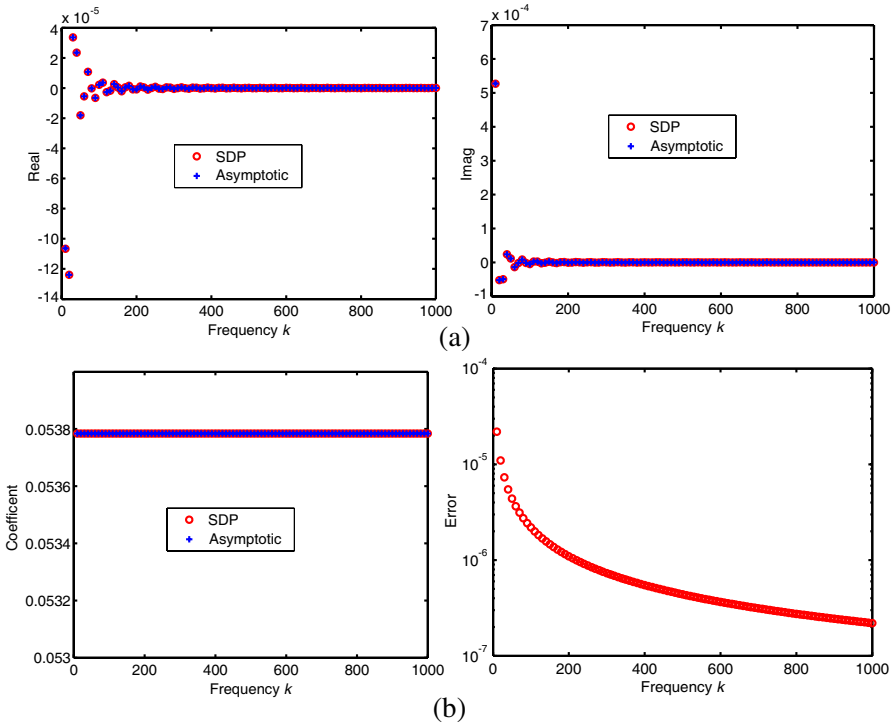

Figure 17. Vertex point $\mathbf{V}_3$: Comparison of the real and imaginary parts of the numerical SDP closed-form formula $I_{\mathbf{V}_3} = I_{L_2}^{(a_3,b_3)} - I_{L_2}^{(a_2,b_2)}$ results (Equations (56)–(57)) by using the asymptotic approximation with leading term $c_0 e^{ik[L_2^2+(a_2L_2+b_2)^2]}/k^2$ [18] (a). Comparison of the coefficients $T_3(k) = |I_{\mathbf{V}_3} \times k^2|$ and $|c_0| = |c_0 e^{ik[L_2^2+(a_2L_2+b_2)^2]}|$. Error $= |T_3(k) - c_0 e^{ik[L_2^2+(a_2L_2+b_2)^2]}|$ (b).

Figure 19 by using the numerical SDP and the traditional asymptotic expansion methods.

Using the brute force method as reference, Figure 20(a) presents the comparison errors between the numerical SDP and asymptotic approximation methods [18]. We see that when k is around 50, the accuracy lost from traditional asymptotic approximation method is about 10^{-2}. However, the computational results accuracy lost by the numerical SDP method is less than 10^{-6}. Hence, the numerical SDP method can significantly improve the PO integral computational results accuracy even when k is not very large.

In Figure 21, the resultant errors of numerical SDP and asymptotic

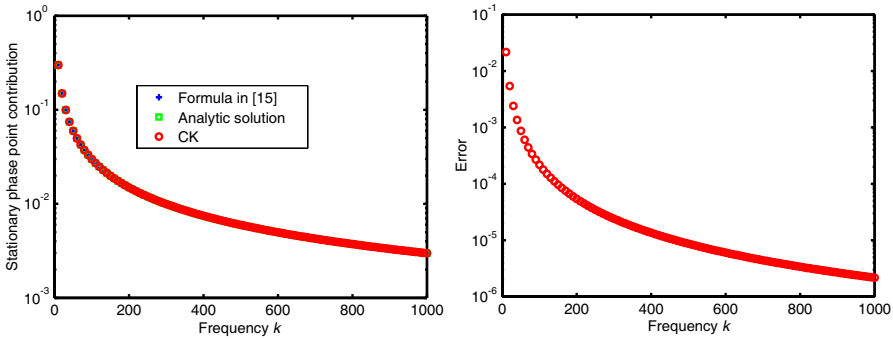

Figure 18. Comparison of the stationary phase point contribution results by three ways: Equation (35) in [18], the derived formula Equation (62) and the numerical SDP method CK given in Equation (85) (a). Comparison of the magnitudes error of the stationary phase point contribution results CK and the asymptotic expansion leading term $J_s = -\frac{\pi}{ik}\alpha_1$ given in Equation (35) [18], Error $= CK - J_s$ (b).

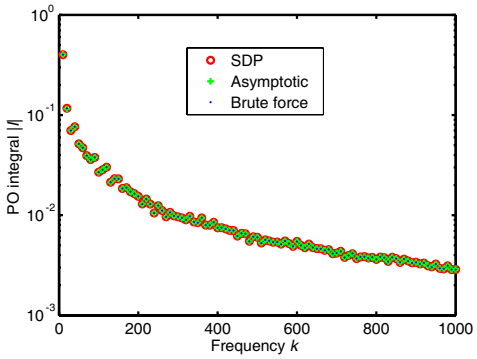

Figure 19. Calculating the PO integral I by using the numerical SDP method Equation (53), the summation of all asymptotic expansion leading terms as shown in [18] and the brute force method.

methods [18] are given to illustrate the accuracy improvement by the numerical SDP method.

In summary, we can see the numerical SDP method is **error-controllable** in accuracy and **frequency-independent** in computational effort based on Figure 20!

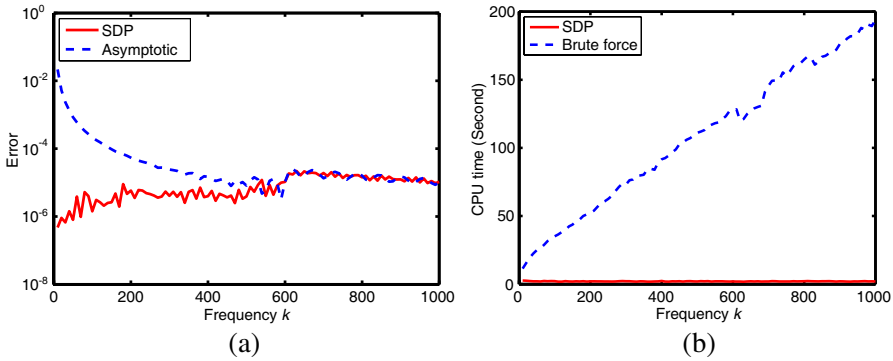

Figure 20. Blue line: The total contribution point results error by using the numerical SDP results Equation (53) relative to the brute force results on the triangular patch. Green line: the error of the summation of the asymptotic leading terms [18] relative to brute force results (a). CPU time comparison by using the numerical SDP and brute force methods (b).

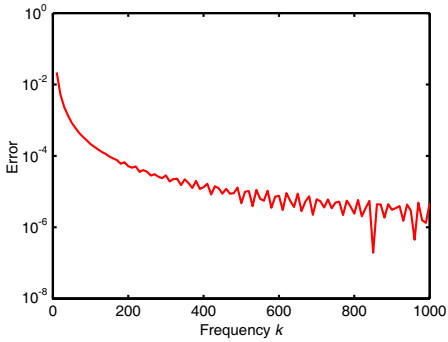

Figure 21. The total contribution point results error between the numerical SDP method Equation (53) and the summation of all asymptotic expansion leading terms on the triangular patch.

6. CONCLUSION

In this paper, we focused on the difficult highly oscillatory PO integral on right-angled trapezoid domains. The two dimensional integral is reduced to line integrals related to complementary error functions. Steepest descent paths deformation on the complex plane are used to calculate the highly oscillatory line integrals. Due to the Stokes' phenomenon of complementary error functions, various formulas of the

PO integrals for different cases will occur and are derived completely. Using the closed-form formula of PO integral on the arbitrary line, we extend the PO integral to triangular patch. Physically, the highly oscillatory PO integral has resonance point, vertex point and stationary point contributions. The numerical SDP formulations are used to compare these contribution point results with the leading terms of traditional asymptotic expansion approximation. When the frequency k is large enough, both methods agree quite well. However, when the frequency is around 20–50, the accuracy lost by using traditional asymptotic expansion method is about one to two digits (10^{-1} to 10^{-2}). Supported by brute force method numerical verifications, the numerical SDP method in this paper provides higher accuracy and error-controllable results even when k is not large. Furthermore, the CPU time consumed by the numerical SDP method is frequency-independent.

ACKNOWLEDGMENT

The authors would like to thank the anonymous reviewers for suggestions to improve this manuscript and to add more material. This work was supported in part by the Research Grants Council of Hong Kong (GRF 711609, 711508, 711511, and 713011), HKU Small Project Funding (201007176196), HKU Seed funding (201102160033), HKU UDF-CSE grant, and in part by the University Grants Council of Hong Kong (Contract No. AoE/P-04/08).

APPENDIX A. DERIVATION OF $F(X)$ IN EQUATION (17)

$$\begin{aligned} F(x) &= \int_0^{ax+b} p(x,y)e^{iky^2}dy = \int_0^{ax+b} \left(\alpha_1+\alpha_2 x+\alpha_4 x^2\right) e^{iky^2}dy \\ &\quad + \int_0^{ax+b} \left(\alpha_3 y+\alpha_6 xy\right) e^{iky^2}dy + \int_0^{ax+b} \left(\alpha_5 y^2\right) e^{iky^2}dy \\ &= F_1(x)+F_2(x)+F_3(x). \end{aligned}$$

After integration by parts, we have the following closed form formulas for $F_m(x)$, $m = 1, 2, 3$:

$$\begin{aligned} F_1(x) &= \int_0^{ax+b} \left(\alpha_1+\alpha_2 x+\alpha_4 x^2\right) e^{iky^2}dy \\ &= -\left(\alpha_1+\alpha_2 x+\alpha_4 x^2\right)\frac{\sqrt{\pi}}{2\sqrt{-ik}}\left(\operatorname{erfc}\left(\sqrt{-ik}(ax+b)\right)-1\right), \end{aligned}$$

$$
\begin{aligned}
F_2(x) &= \int_0^{ax+b} (\alpha_3 y + \alpha_6 xy)\, e^{iky^2} dy \\
&= \frac{\alpha_3 + \alpha_6 x}{2jk} \left(e^{ik(ax+b)^2} - 1 \right), \\
F_3(x) &= \int_0^{ax+b} (\alpha_5 y^2) e^{iky^2} dy \\
&= \frac{\alpha_5 (ax+b)}{2ik} e^{ik(ax+b)^2} + \frac{\alpha_5 \sqrt{\pi}}{4i(ik)^{\frac{3}{2}}} \left(\operatorname{erfc}\left(\sqrt{-ik}(ax+b) \right) - 1 \right).
\end{aligned}
$$

Summing the above three equations, we have

$$
\begin{aligned}
F(x) &= F_1(x) + F_2(x) + F_3(x) \\
&= -\left(\alpha_1 + \alpha_2 x + \alpha_4 x^2 - \frac{\alpha_5}{2ik} \right) \frac{\sqrt{\pi}}{2\sqrt{-ik}} \left(\operatorname{erfc}\left(\sqrt{-ik}(ax+b) \right) - 1 \right) \\
&\quad + \frac{\alpha_3 + \alpha_6 x + \alpha_5 (ax+b)}{2ik}\, e^{ik(ax+b)^2} - \frac{\alpha_3 + \alpha_6 x}{2ik}.
\end{aligned}
$$

APPENDIX B. CLOSED-FORM FORMULA CASES FOR I_2^{ANALYTIC}

From Stokes line formula Equation (26), after substituting $z = ax+b$ on the complex plane, we can see $(x_0, 0) = (-\frac{b}{a}, 0)$ is the intersection point between the Stokes line $l(z)$ and the real x axis. From Cauchy's integral theorem, the following (Figures 5–6) are all the cases for I_2^{analytic}:
(1) $L_1 < x_s < L_2$ and $x_0 < L_1$ (Figure 5(a)),
when $a > 0$,

$$
I_2^{\text{analytic}} = \int_{\mathbf{A}}^{\mathbf{B}} 2j_1(x) e^{ikx^2} dx = K(\mathbf{B}) - K(\mathbf{A}),
$$

when $a < 0$,

$$
\begin{aligned}
I_2^{\text{analytic}} &= \int_{(L_1,0)}^{(L_2,0)} 2j_1(x) e^{ikx^2} dx - \int_{\mathbf{A}}^{\mathbf{B}} 2j_1(x) e^{ikx^2} dx \\
&= K((L_2,0)) - K((L_1,0)) - K(\mathbf{B}) + K(\mathbf{A}).
\end{aligned}
$$

(2) $L_1 < x_s < L_2$ and $L_1 < x_0 < x_s$ (Figure 5(b)),
when $a > 0$,

$$
\begin{aligned}
I_2^{\text{analytic}} &= \int_{(L_1,0)}^{(x_0,0)} 2j_1(x) e^{ikx^2} dx + \int_{(x_0,0)}^{\mathbf{B}} 2j_1(x) e^{ikx^2} dx \\
&= K(\mathbf{B}) - K((L_1,0)).
\end{aligned}
$$

when $a < 0$,

$$I_2^{\text{analytic}} = \int_{\mathbf{B}}^{(L_2,0)} 2j_1(x)e^{ikx^2}dx = K((L_2,0)) - K(\mathbf{B}).$$

(3) $L_1 < x_s < L_2$ and $x_s < x_0 < L_2$ (Figure 5(c)),
when $a > 0$,

$$\begin{aligned} I_2^{\text{analytic}} &= \int_{(L_1,0)}^{(x_s,0)} 2j_1(x)e^{ikx^2}dx + \int_{(x_s,0)}^{\mathbf{A}} 2j_1(x)e^{ikx^2}dx \\ &= K(\mathbf{A}) - K((L_1,0)), \end{aligned}$$

when $a < 0$,

$$I_2^{\text{analytic}} = \int_{\mathbf{A}}^{(L_2,0)} 2j_1(x)e^{ikx^2}dx = K((L_2,0)) - K(\mathbf{A}).$$

(4) $L_1 < x_s < L_2$ and $x_s < x_0 < L_2$ (Figure 5(d)),
when $a > 0$,

$$\begin{aligned} I_2^{\text{analytic}} &= \int_{(L_1,0)}^{\mathbf{A}} 2j_1(x)e^{ikx^2}dx + \int_{\mathbf{B}}^{(L_2,0)} 2j_1(x)e^{ikx^2}dx. \\ &= K(\mathbf{A}) - K((L_1,0)) + K((L_2,0)) - K(\mathbf{B}), \end{aligned}$$

when $a < 0$,

$$I_2^{\text{analytic}} = \int_{\mathbf{A}}^{\mathbf{B}} 2j_1(x)e^{ikx^2}dx = K(\mathbf{B}) - K(\mathbf{A}).$$

(5) $L_1 > x_s$ and $x_0 < L_1$ (Figure 6(a)),
when $a > 0$,

$$I_2^{\text{analytic}} = 0,$$

when $a < 0$,

$$I_2^{\text{analytic}} = K((L_2,0)) - K((L_1,0)).$$

(6) $L_1 > x_s$ and $L_1 < x_0 < L_2$ (Figure 6(b)),
when $a > 0$,

$$I_2^{\text{analytic}} = \int_{(L_1,0)}^{\mathbf{A}} 2j_1(x)e^{ikx^2}dx = K(\mathbf{A}) - K((L_1,0)),$$

when $a < 0$,

$$I_2^{\text{analytic}} = \int_{\mathbf{A}}^{(L_2,0)} 2j_1(x)e^{ikx^2}dx = K((L_2,0)) - K(\mathbf{A}).$$

(7) $L_1 > x_s$, $L_2 < x_0$ (Figure 6(c)),
when $a > 0$,

$$I_2^{\text{analytic}} = \int_{(L_1,0)}^{\mathbf{A}} 2j_1(x)e^{ikx^2}dx + \int_{\mathbf{B}}^{(L_2,0)} 2j_1(x)$$
$$= K(\mathbf{A}) - K((L_1,0)) + K((L_2,0)) - K(\mathbf{B}),$$

when $a < 0$,

$$I_2^{\text{analytic}} = \int_{\mathbf{A}}^{\mathbf{B}} 2j_1(x)e^{ikx^2}dx = K(\mathbf{B}) - K(\mathbf{A}).$$

(8) $L_2 < x_s$, $x_0 < L_1$ (Figure 6(d)),
when $a > 0$,

$$I_2^{\text{analytic}} = \int_{(L_1,0)}^{\mathbf{A}} 2j_1(x)e^{ikx^2}dx + \int_{\mathbf{B}}^{(L_2,0)} 2j_1(x)$$
$$= K(\mathbf{A}) - K((L_1,0)) + K((L_2,0)) - K(\mathbf{B}),$$

when $a < 0$,

$$I_2^{\text{analytic}} = \int_{\mathbf{A}}^{\mathbf{B}} 2j_1(x)e^{ikx^2}dx = K(\mathbf{B}) - K(\mathbf{A}).$$

(9) $L_2 < x_s$, $L_1 < x_0 < L_2$ (Figure 6(e)),
when $a > 0$,

$$I_2^{\text{analytic}} = \int_{(L_1,0)}^{\mathbf{B}} 2j_1(x)e^{ikx^2}dx = K(\mathbf{B}) - K((L_1,0)),$$

when $a < 0$,

$$I_2^{\text{analytic}} = \int_{\mathbf{B}}^{(L_2,0)} 2j_1(x)e^{ikx^2}dx = K((L_2,0)) - K(\mathbf{B}).$$

(10) $L_2 < x_s$, $x_0 < L_1$ (Figure 6(f)),
when $a > 0$,

$$I_2^{\text{analytic}} = \int_{(L_1,0)}^{(L_2,0)} 2j_1(x)e^{ikx^2}dx = K((L_2,0)) - K((L_1,0)),$$

when $a < 0$,

$$I_2^{\text{analytic}} = 0.$$

REFERENCES

1. Chew, W. C., *Waves and Fields in Inhomogeneous Media*, IEEE Press, New York, 1995.
2. Knott, E. F., J. F. Shaeffer, and M. T. Tuley, *Radar Cross Section*, Artech House, Norwood, 1993.
3. Ufimtsev, P. Y., *Fundamentals of the Physical Theory of Diffraction*, John Wiley and Sons, Inc., New York, 2007.
4. Macdonald, H. M., "The effect produced by an obstacle on a train of electric waves," *Phil. Trans. Royal Soc. London, Series A, Math. Phys. Sci.*, Vol. 212, 299–337, 1913.
5. Ludwig, A. C., "Computation of radiation patterns involving numerical double integration," *IEEE Trans. Antennas Propag.*, Vol. 16, No. 6, 767–769, Nov. 1968.
6. Gordon, W. B., "Far-field approximations to the Kirchhoff-Helmholtz representation of scattered fields," *IEEE Trans. Antennas Propag.*, Vol. 23, No. 4, 590–592, Jul. 1975.
7. Gordon, W. B., "High-frequency approximations to the physical optics scattering integral," *IEEE Trans. Antennas Propag.*, Vol. 42, No. 3, 427–432, Mar. 1994.
8. Bolukbas, D. and A. A. Ergin, "A radon transform interpretation of the physical optics integral," *Microw. Opt. Tech. Lett.*, Vol. 44, No. 3, 284–288, Feb. 2005.
9. Serim, H. A. and A. A. Ergin, "Computation of the physical optics integral on NURBS surfaces using a radon transform interpretation," *IEEE Antennas Wireless Propag. Lett.*, Vol. 7, 70–73, 2008.
10. Ulku, H. A. and A. A. Ergin, "Radon transform interpretation of the physical optics integral and application to near and far field acoustic scattering problems," *IEEE Antennas and Propagation Society International Symposium, APSURSI*, 2010.
11. Infante, L. and M. Stefano, "Near-field line-integral representation of the Kirchhoff-type aperture radiation for parabolic reflector," *IEEE Antennas Wireless Propag. Lett.*, Vol. 2, No. 1, 273–276, 2003.
12. Burkholder, R. J. and T. H. Lee, "Adaptive sampling for fast physical optics numerical integration," *IEEE Trans. Antennas Propag.*, Vol. 53, No. 5, 1843–1845, May 2005.
13. Conde, O. M., J. Pérez, and M. F. Cátedra, "Stationary phase method application for the analysis of radiation of complex 3-D conducting structures," *IEEE Trans. Antennas Propag.*, Vol. 49,

No. 5, 724–731, May 2001.

14. Cátedra, M. F., C. Delgado, S. Luceri, O. G. Blanco, and F. S. Adana, "Physical optics analysis of multiple interactions in large scatters using current modes," *IEEE Trans. Antennas Propag.*, Vol. 54, No. 3, 985–994, Mar. 2006.
15. Delgado, C., J. M. Gómez, and M. F. Cátedra, "Analytical field calculation involving current modes and quadratic phase expressions," *IEEE Trans. Antennas Propag.*, Vol. 55, No. 1, 233–240, Jan. 2007.
16. Cátedra, M. F., C. Delgado, and I. G. Diego, "New physical optics approach for an efficient treatment of multiple bounces in curved bodies defined by an impedance boundary condition," *IEEE Trans. Antennas Propag.*, Vol. 56, No. 3, 728–736, Mar. 2008.
17. Vico, F., M. Ferrando, and A. Valero, "A new fast physical optics for smooth surfaces by means of a numerical theory of diffraction," *IEEE Trans. Antennas Propag.*, Vol. 58, No. 3, 773–789, Mar. 2010.
18. Carluccio, G., M. Albani, and P. H. Pathak, "Uniform asymptotic evaluation of surface integrals with polygonal integration domains in terms of UTD transition functions," *IEEE Trans. Antennas Propag.*, Vol. 58, No. 4, 1155–1163, Apr. 2010.
19. Albani, M., G. Carluccio, and P. H. Pathak, "Uniform ray description for the PO scattering by vertices in curved surface with curvilinear edges and relatively general boundary conditions," *IEEE Trans. Antennas Propag.*, Vol. 59, No. 5, 1587–1596, May 2011.
20. Harrington, R., *Field Computation by Moment Method*, Macmillan, New York, 1968.
21. Borovikov, V. A., *Uniform Stationary Phase Method*, Institution of Electrical Engineers, London, 1994.
22. James, G. L., *Geometrical Theory of Diffraction for Electromagnetic Waves*, Peregrinus, Stevenage, 1980.
23. Langdon, S. and S. N. Chandler-Wilde, "A wavenumber independent boundary element method for an acoustic scattering problem," *SIAM J. Numer. Anal.*, Vol. 43. No. 6, 2450–2477, 2006.
24. Bruno, O. P., C. A. Geuzaine, J. A. Monro, Jr., and F. Reitich, "Prescribed error tolerances within fixed computational times for scattering problems of arbitrarily high frequency: The convex case," *Phil. Trans. Royal Soc. London, Series A*, Vol. 362, 629–645, 2004.

25. Geuzaine, C., O. Bruno, and F. Reitich, "On the $O(1)$ solution of multiple-scattering problems," *IEEE Trans. Magn.*, Vol. 41, No. 5, 1498–1491, May 2005.
26. Bruno, O. P. and C. A. Geuzaine, "An $O(1)$ integration scheme for three-dimensional surface scattering problems," *J. Comp. Appl. Math.*, Vol. 204, No. 2, 463–476, 2007.
27. Engquist, B., E. Fatemi, and S. Osher, "Numerical solution of the high frequency asymptotic expansion for the scalar wave equation," *J. Comput. Phys.*, Vol. 120. No. 1, 145–155, Aug. 1995.
28. Engquist, B. and O. Runborg, "Multi-Phase computations in geometrical optics," *J. Comp. Appl. Math.*, Vol. 74, No. 1–2, 175–192, 1996.
29. Engquist, B. and O. Runborg, "Computational high frequency wave propagation," *Acta Numerica*, Vol. 12, 181–266, 2003.
30. Iserles, A. and S. P. Nøsett, "Quadrature methods for multivariate highly oscillatory integrals using derivatives," *Math. Comp.*, Vol. 75, No. 255, 1233–1258, 2006.
31. Iserles, A. and S. P. Nøsett, "On the computation of highly oscillatory multivariate integrals with critical points," *BIT*, Vol. 46, No. 3, 549–566, 2006.
32. Iserles, A. and S. P. Nøsett, "From high oscillation to rapid approximation III: Multivariate expansions," *IMA J. Num. Anal.*, Vol. 29, No. 4, 882–916, 2009.
33. Iserles, A. and D. Levin, "Asymptotic expansion and quadrature of composite highly oscillatory integrals," *Math. Comp.*, Vol. 80, No. 273, 279–296, 2011.
34. Huybrechs, D. and S. Vandewalle, "The construction of cubature rules for multivariate highly oscillatory integrals," *Math. Comp.*, Vol. 76, No. 260, 1955–1980, 2007.
35. Huybrechs, D. and S. Vandewalle, "A sparse discretisation for integral equation formulations of high frequency scattering problems," *SIAM J. Sci. Comput.*, Vol. 29, No. 6, 2305–2328, 2007.
36. Asheim, A. and D. Huybrechs, "Asymptotic analysis of numerical steepest descent with path approximations," *Found. Comput. Math.*, Vol. 10, No. 6, 647–671, 2010.
37. Asheim, A., "Numerical methods for highly oscillatory problems," Ph.D. Dissertation, Norwegian University of Science and Technology, Department of Mathematical Sciences, 2010.
38. Wong, R., *Asymptotic Approximations of Integrals*, SIAM, New York, 2001.

39. Kouyoumjian, R. G. and P. H. Pathak, "A uniform geometrical theory of diffraction for an edge in a perfectly conducting surface," *Proceedings of the IEEE*, Vol. 62, No. 11, 1448–1461, Nov. 1974.
40. Lee, S. W. and G. A. Deschamps, "A uniform asymptotic theory of electromagnetic diffraction by a curved wedge," *IEEE Trans. Antennas Propag.*, Vol. 24, No. 1, 25–34, Jan. 1976.
41. Ikuno, H. and M. Nishimoto, "Calculation of transfer functions of three-dimensional indented objects by the physical optics approximation combined with the method of stationary phase," *IEEE Trans. Antennas Propag.*, Vol. 39, No. 5, 585–590, May 1991.
42. Jones, D. S. and M. Kline, "Asymptotic expansion of multiple integrals and the method of stationary phase," *J. Math. Phys.*, Vol. 37, 1–28, 1958.
43. Chako, N., "Asymptotic expansions of double and multiple integral," *J. Inst. Math. Applic.*, Vol. 1, No. 4, 372–422, 1965.
44. Davis, C. P. and W. C. Chew, "Frequency-independent scattering fom a flat strip with TE_z-polarized fields," *IEEE Trans. Antennas Propag.*, Vol. 56, No. 4, 1008–1016, Apr. 2008.
45. Sha, W. E. I. and W. C. Chew, "High frequency scattering by an impenetrable sphere," *Progress In Electromagnetics Research*, Vol. 97, 291–325, 2009.
46. Abramowitz, M. and I. A. Stegun, *Handbook of Mathematical Functions*, Norwood, MA, Dover, 1972.
47. Josef, S. and B. Roland, *Introduction to Numerical Analysis*, Springer-Verlag, New York, 1980.